ACS APPLIED BIO MATERIALS

www.acsabm.org Article

Visible Light-Activated Water-Soluble Platicur Nanocolloids: Photocytotoxicity and Metabolomics Studies in Cancer Cells

Federica De Castro, Viviana Vergaro,* Michele Benedetti, Francesca Baldassarre, Laura Del Coco, Maria Michela Dell'Anna, Piero Mastrorilli, Francesco Paolo Fanizzi,* and Giuseppe Ciccarella*

Cite This: *ACS Appl. Bio Mater.* 2020, 3, 6836–6851 Read Online

ACCESS | Metrics & More | Article Recommendations | Supporting Information

ABSTRACT: Nanoparticle-based drug delivery systems for cancer therapy offer a great promising opportunity as they specifically target cancer cells, also increasing the bioavailability of anticancer drugs characterized by low water solubility. Platicur, [Pt(cur) $(NH_3)_2$](NO_3), is a *cis*-diamine−platinum(II) complex linked to curcumin. In this work, an ultrasonication method, coupled with layer by layer technology, allows us to obtain highly aqueous stable Platicur nanocolloids of about 100 nm. The visible light-activated Platicur nanocolloids showed an increased drug release and antitumor activity on HeLa cells, with respect to Platicur nanocolloids in darkness. This occurrence could give very interesting insight into selective activation of the nanodelivered Pt(II) complex and possible side-effect lowering. For the first time, the metabolic effects of Platicur nanocolloid photoactivation, in the HeLa cell line, have been investigated using an NMR-based metabolomics approach coupled with statistical multivariate data analysis. The reported results highlight specific metabolic differences between photoactivated and non-photoactivated Platicur NC-treated HeLa cancer cells.

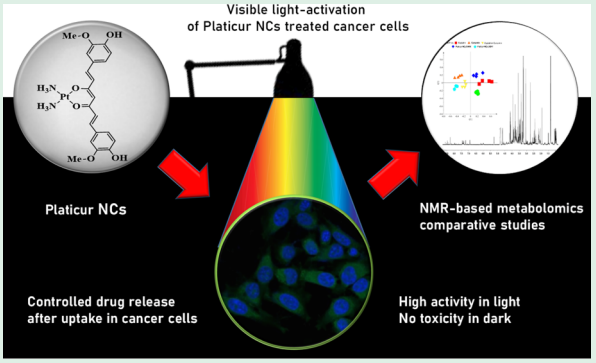

KEYWORDS: *photoactivated chemotherapy, nanocolloids, metal complexes, platinum complexes, curcumin, NMR metabolomics*

INTRODUCTION

Over the last decade, radiation, chemotherapy, and surgery have become the typical cancer treatment protocols in oncological patients.[1−3] On the other hand, all three methods risk damaging normal tissues or lead to incomplete eradication of the cancer. Among these protocols, chemotherapy remains the most significant treatment, with cisplatin being the most potent chemotherapeutic drug used for different kinds of tumors.[1−5] Despite the considerable properties of cisplatin, its use often leads to several side effects and the onset of resistance phenomena in treated patients, thus leading to treatment failure. These problems are mainly due to non-specific interactions of the drug with noncancerous cells in the body and onset of escape pathways that cancer cells follow to resist and evade treatments.[5]

In order to overcome these disadvantages, many research studies are devoted to synthesize and study new cisplatin analogues and new strategies have been developed focusing selective targets and/or specific activation of the antitumor drugs.[1,2,5−8] A new class of platinum drugs includes photo-activable prodrugs allowing the increase in selectivity, hence lowering toxicity. These compounds could find use in treating all localized tumors such as many solid tumors (*e.g.*, esophagus, head and neck, lung, bladder, cervix, and colon) growing in body cavities accessible by specific devices.[8] Selectivity of pharmacological action is of key importance for successful drug therapy.[5,8] Low selectivity toward tumor cells leads to high toxicity and serious side effects. Phototherapy is a promising methodology to treat cancer because it reduces the side effects of conventional systemic chemotherapies.[8] In general, the hypoxic is related to many tumors and photoactive molecules are usually less effective under low-oxygen conditions.[9] For this reason, complexes based on platinum[10] and rhodium[11] offering the possibility of oxygen-independent photo-chemotherapy are particularly attractive.[12] Ideally, the platinum prodrug should be selectively accumulated by cancer with respect to normal cells and characterized by a large difference between the light and dark toxicity.[8] Despite being a young field, the development of photoactivatable platinum complexes already produced a wealth of interesting results.[8] Recently, a *cis*-diamine−platinum(II) complex linked to curcumin (cur), Platicur, [Pt(cur) $(NH_3)_2$](NO_3), has been synthesized.[13] Platicur is a new Pt(II) complex in which cur, binding to the

Received: June 22, 2020
Accepted: September 7, 2020
Published: September 7, 2020

https://dx.doi.org/10.1021/acsabm.0c00766
ACS Appl. Bio Mater. 2020, 3, 6836−6851

metal in its enolic form, confers to the complex photosensitive properties. As other natural compounds obtained from plants, cur gained considerable attention in the scientific community as a chemotherapeutic agent also for its nontoxic nature and the correlated lowering of side effects compared to other chemotherapeutic drugs.[14] The main limits of cur are its poor water solubility (<0.1 mg/mL)[15] and its rapid degradation, which lead to poor bioavailability and pharmacokinetics.[13,15] As reported in the literature, the degradation of cur can be reduced upon its complexation with d- and f-block metal ions.[13,16] When cur binds to the metal, the obtained complex improves its water solubility.[13,16,17] Mitra *et al.* have demonstrated how the photoactivation of Platicur was accountable for the production of both active species of Pt(II) and photoactive cur (Scheme S1), resulting in a synergic dual action mechanism and an interesting anticancer activity.[13] Some research groups have tried to improve the therapeutic efficacies and solubility of cur using a drug delivery system.[18,19] Codelivering of the platinum complex and cur has also been used in order to improve drug efficacy.[20] No previous attempts of the delivery of both cur and a cisplatin analogue from a single prodrug are reported in the literature before the present study. Platicur is soluble only in organic solvents, so in this work, an ultrasonication method, coupled with layer by layer technology (LbL), was exploited to produce aqueous-stable nanocolloids of Platicur (Platicur-NCs).[21,22] Wrapping drug nanoparticles with polymers is one of the best approaches for the preparation of nanocarriers with high payload of the active drug and controlled release kinetics.[23−26] The ultrasonication, applied in the presence of a charged polymer, forms a charged layer around the particle surface, stabilizing the colloidal suspension and preventing fast particle aggregation. After the sonication treatment, the obtained NCs are encapsulated according to the (LbL) technology using an opposite-charged polymer. In this work, chitosan and pectin polysaccharides were chosen for design of the drug delivery systems obtaining NCs of about 100 nm. In the literature, there are few studies which reported chitosan−pectin LbL complexes used as carriers for cancer therapy.[27]

Nanocarriers enable controlled drug release, resulting in increased selectivity toward tumors and reduced toxicity, becoming a promising approach for cancer treatment.[7] Moreover, their use overcomes problems related to the scarce aqueous solubility of chemotherapeutic drugs, enhancing their specific targeting to tumor tissues and reducing adverse side effects to healthy ones.[6,7,28] Because of their size and surface chemical properties, nanocarriers could also increase the delivered overall therapeutic index of drugs. This may occur through nanoformulations in which chemotherapeutics are either encapsulated or conjugated to the surfaces of nanoparticles. Size represents the key point in the delivery of nanotechnology-based therapeutics to tumor tissues. Indeed, the increased permeability of tumor vasculature allows nanoparticles (<200 nm) to accumulate in the tumor microenvironment. Moreover, the drug release, according to material composition, can be controlled by triggered events, such as ultrasound, pH, and heat.[9,19,28,29]

The use of Platicur NCs allows controlled active drug release making photo-chemotherapy more advantageous in contrast to the conventional anticancer therapies.[30,31] The here-reported study has been conceptualized with the idea that nanoformulation should be stable under physiological conditions and nontoxic in the darkness. The new Platicur NCs have been characterized for their physical chemical properties, the loading and release efficiency, and the biological activity in model cancer cells. In order to study the drug effects, we also found defining the metabolic profiling of cultured cells essential.[3−5,32] Interestingly, no metabolomics study of photoactivated nanoplatinum complexes on tumor cell lines and of the effects of photoactivation on cancer cells has been previously reported. Therefore, in this work, a ^{1}H NMR metabolomics approach was used to detect variations in small metabolites and mobile lipids upon exposure of the HeLa cancer cell line (cervix cancer cell line) to photoactivated Platicur NCs. ^{1}H NMR spectroscopy is one of the most powerful techniques to characterize the metabolome of culture cell lines because it allows nondestructive and rapid screening of the major metabolites involved in specific metabolic pathways.[33] HeLa cells were treated at the respective IC_{50} dose and the 24 h overexposure was followed, in order to highlight the pattern of variation and/or correlation according to the used drugs. The NMR data for photoactivated Platicur NC treatement were compared with those obtained for cisplatin, cur, cisplatin and cur (cotreatment), and non-photoactivated Platicur NCs. Platicur NCs showed, in addition to an enhanced drug solubility, an improvement in their pharmacological activity because of the possibility of photoactivation control.

EXPERIMENTAL SECTION

Synthesis of Complexes. All solvents and reagents including cisplatin were purchased from Aldrich Chemical Company and used as received, except otherwise stated. Chitosan (CHI, medium molecular weight, 448,877) and low-methoxyl pectin (PEC LM 38% degree of esterification, CU701, lot 968, from citrus fruits) were kindly provided by Herbstreith & Fox (Neuemberg, Germany). Platicur was synthetized according to the procedure described by Censi *et al.*[17]

Synthesis of Platicur NCs. A sonication-assisted LbL technique was used to prepare the NCs, using a VC 750 HV Sonics ultrasonicator. Biodegradable polymers, chitosan (polycation) and pectin (polyanion), were chosen for coating LbL technology. Specifically, Platicur (2.0 mg) was added to 10 mL of solution containing chitosan 0.1% and acetic acid 0.5%, stirred for 5 min, and then ultrasonicated at 20% of power (150 Watt) in a water/ice bath for 20 min to obtain Platicur/chitosan nanocores. The LbL self-assembly of pectin and chitosan was then performed using the LbL method, as reported in our previous work.[25] The procedure was repeated for each polyelectrolyte, resulting in the deposition of five polyelectrolyte layers on the Platicur NCs.

NC Characterization. TEM images were collected with a JEOL JEM 1400 with a LaB6 source at 80 kV so as not to damage the organic coating. Scanning transmission electron microscopy (STEM) imaging was recorded using a FE-SEM microscope (Carl Zeiss Merlin), equipped with a Gemini II column, with a complete high angle annular and annular dark field/bright field STEM detector system and with a FEG source operating at an accelerating voltage of 20 kV and with short exposure time of a few seconds to minimize sample damages.

The zeta potential and the hydrodynamic diameter of NCs were measured with a Malvern Zetasizer Nano ZS.

The optical measurements, UV−vis absorption and emission spectra, were obtained on a Varian- Cary 500 spectrophotometer and Varian Cary Eclipse spectrofluorimeter, respectively. Absorption and fluorescence spectra were measured in distilled water, with a final concentration of 50 μM. The quartz cuvettes used were of 1.0 cm path length.

Platinum Quantification in NCs by ICP. Drug loading was calculated by ICP. The experimental setup provides the construction of a calibration line, using four points. Loading percentage is defined as the ratio of platinum concentration (ng/L) in solution after and

https://dx.doi.org/10.1021/acsabm.0c00766
ACS Appl. Bio Mater. 2020, 3, 6836−6851

before drug loading. ICP experiments were performed with a ICP-OES Thermo Scientific.

Release Kinetics. The release kinetics was evaluated in phosphate buffer at physiological pH by ICP, as reported in our study.[25]

Incubation and Staining of Living Cells. The HeLa cancer cell line was maintained in Dulbecco's modified Eagle's medium supplemented with fetal bovine serum (10%), penicillin (100 U mL^{-1} culture medium), streptomycin (100 mg mL^{-1} culture medium), and glutamine (5%). Cells were grown in a humidified incubator at 37 °C, 5% CO_2, and 95% relative humidity. The cell line was serum-starved for 24 h before any test. For staining experiments, HeLa (5×10^4) cells were seeded onto a 35 mm glass-bottom Petri dish and incubated in complete media for 24 h. Then, the cells were incubated with cur and Platicur NCs (50 μM) for 30 min or 2 h in the dark in a humidified incubator at 37 °C, 5% CO_2, and 95% relative humidity. The preparation of samples for confocal imaging was previously reported.[25]

Cytotoxicity Determination by the MTT Method. The HeLa cancer cell line was used in the general cytotoxicity test. The MTT method was used to measure the activity of living cells via mitochondrial dehydrogenase activity, as already reported.[25]

Confocal Imaging of Living Cells. Biological imaging tests were carried out with a Zeiss LSM700 confocal laser scanning microscope (Zeiss, Germany) equipped with a Zeiss Axio Observer Z1 inverted microscope using a 63× objective with a 1.46 numerical aperture oil immersion lens for imaging. Laser beams with 405 nm and 488 nm excitation wavelengths (0.5 mW) were used for Hoechst and cur or Platicur NC imaging, respectively. The fluorescence of cur or Platicur NCs was collected through the FITC filter (excitation wavelength: 488 nm). The fluorescence intensity of samples was calculated from the microscopic images using the software Zen 2009.

DCFDA Assay. DCFDA assay was used to detect generation of cellular reactive oxygen species (ROS). DCFDA on oxidation by cellular ROS generates fluorescent DCF having the emission spectral maximum at 525 nm. The percentage of cell population generating ROS was determined by fluorescence-activated cell sorting (FACS). About 3.0×10^5 HeLa cells were plated in two 6-well plates and treated with compounds [cisplatin, 35 μM; cur, 90 μM; and Platicur NCs, 75 μM or 50 nM] and incubated for 4 h in the dark. One plate was irradiated with visible light of 400−700 nm for 1 h in PBS, while the other was kept in the dark. The cells were subsequently trypsinized and a clear suspension of $\sim 10^5$ cells mL^{-1} was made. The suspensions were then treated with 1.0 μM DCFDA solution and kept in the dark for ∼10 min at room temperature. The samples along with untreated controls were analyzed by FACS. The experiment was performed in duplicates to confirm the results.

Visible Light Irradiation. The samples were put in a flat-bottom 6-well microplate above the xenon lamp (Spectral Products mod. 1118263) for 1 h (at a distance of 3.5 cm). During the irradiation, the temperature was 23 ± 2 °C. Native samples to be irradiated were obtained from the same stock. After irradiations, the samples were kept in the CO_2 incubator for 12 h at 37 °C before further analysis.

Stability of Platicur NCs under Storage Conditions. Platicur NCs were stored at 4 °C in the dark. The stability was checked as reported previously,[34] measuring the variations in the particle size and PDI.

Statistical Analysis. Statistical differences between controls and drug-treated cells were determined by one-way ANOVA (Sidak). *P*-values < 0.05 were considered statistically significant. Data were analyzed using the Stata 8.2/SE package (StataCorp LP).

Cell Sampling for NMR. HeLa cells for NMR metabolomics analyses were cultured to a confluence of 70% (ca 1.5×10^6 cells/flask). The next day, the fresh culture medium was supplemented with the half-maximal inhibitor concentration (IC_{50}) at 24 h (drug concentration causing 50% of cell death) of cisplatin, cur, cisplatin plus cur, non-photoactivated Platicur nanocolloids (Platicur NCs DARK), and photoactivated Platicur nanocolloids (Platicur NCs LIGHT). For control cells, fresh medium without the drug was added. Cells incubated for 24 h were then harvested by tripsinization, washed with PBS, and pelleted by centrifugation (1000 rpm × 10 min). For each condition, four independent assays were performed.

NMR samples were prepared from pelleted HeLa cells (polar and lipophilic metabolites were extracted) and from each respective recovered culture medium, according to the literature.[3,35]

NMR Measurements. All measurements were performed on a Bruker AVANCE III 600 Ascend NMR spectrometer (Bruker, Ettlingen, Germany), operating at 600.13 MHz for ^1H observation, equipped with a TCI cryoprobe incorporating a *z*-axis gradient coil and automatic tuning/matching. Experiments were acquired at 300 K in the automation mode. For each aqueous extract, lipid extract, and culture medium sample, the spectral acquisition parameters were fixed and optimized as reported in the literature.[3]

Metabolite identifications were carried out from 1D and 2D NMR profiles using the associated database of pure compounds and the human metabolome database and ChenomX NMR Suite 8 (ChenomX Inc., Edmonton, Canada) software with comparison with other published data.[36] The NMR spectra were processed using Topspin 3.6.1 and Amix 3.9.13 (Bruker, BioSpin, Italy), for the visual inspection and the bucketing process for the further multivariate statistical analyses.

MVA of NMR Spectra. The ^1H NMR chemical shifts for detected metabolites are reported in Table S1. The bucketing preprocessing procedure was applied on the CMPG spectra, for both aqueous extracts and culture media, and on the ZG spectra, for lipid extracts, covering the range 10.0−0.5 ppm. Each NMR spectrum was automatically divided into rectangular buckets of fixed 0.04 ppm width and integrated using Bruker Amix 3.9.13 software (Bruker, BioSpin). The spectral regions between 5.10 and 4.7 ppm (containing the residual peak from the suppressed water resonance) for aqueous extracts and culture media and between 7.60−7.00 and 3.60−3.00 ppm (containing signals of chloroform and its carbon satellites and the residual methanol, respectively) were excluded. The remaining buckets were normalized to the total area to minimize small differences and subsequently mean-centered. Multivariate statistical analyses (unsupervised principal component analysis (PCA) and the supervised orthogonal partial least squares discriminant analyses, OPLS-DA) were performed to examine the intrinsic variation in the data, using SIMCA 14 software (Sartorius Stedim Biotech, UmeÅ, Sweden).[37] The Pareto scaling procedure was performed by dividing the mean-centered data by the square root of the standard deviation.[38,39] The robustness of the statistical models was tested by the cross-validation default method (7-fold) and further evaluated with a permutation test (100 permutations).[37] The total variations in the data and the internal cross-validation, thus the quality of the statistical models, were described with R^2(cum) and Q^2(cum) parameters and *p* values (p[CV-ANOVA] (a *p*-value of < 0.05, confidence level of 95%, was considered statistically significant) obtained from analysis of variance testing of cross-validated predictive residuals (CV-ANOVA).[32,35,39]

Variations in the metabolite contents between the different conditions of treatments were calculated as the $-\text{Log}_2$ fold change (FC) ratio of the normalized median intensity for the distinctive metabolite signals in the spectra, corresponding to the discussed conditions. The statistical significance of the means of the pairwise groups was obtained using the two-sample *t*-test (a *p*-value of < 0.05 was considered for statistical variance).

Metabolic Pathway Analysis. MetaboAnalyst software[40] was used to identify the metabolic pathways altered (comparison with controls) after the different drug administration on HeLa cells. Metabolites of interest were quantified using selected NMR signals (indicated in Table S1) and were used for the metabolic pathway analysis. The pathway impact was calculated as reported in the literature.[32]

RESULTS AND DISCUSSION

Physical and Chemical Characterization. The ultrasonication-assisted LbL assembly process allowed us to obtain stable nanocores of Platicur starting from drug microcrystals.

https://dx.doi.org/10.1021/acsabm.0c00766
ACS Appl. Bio Mater. 2020, 3, 6836−6851

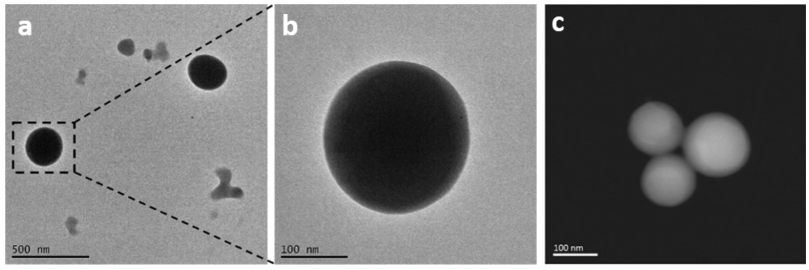

Figure 1. TEM (a,b) and STEM (c) characterization of Platicur NCs obtained after 20 min of ultrasonication in chitosan solution.

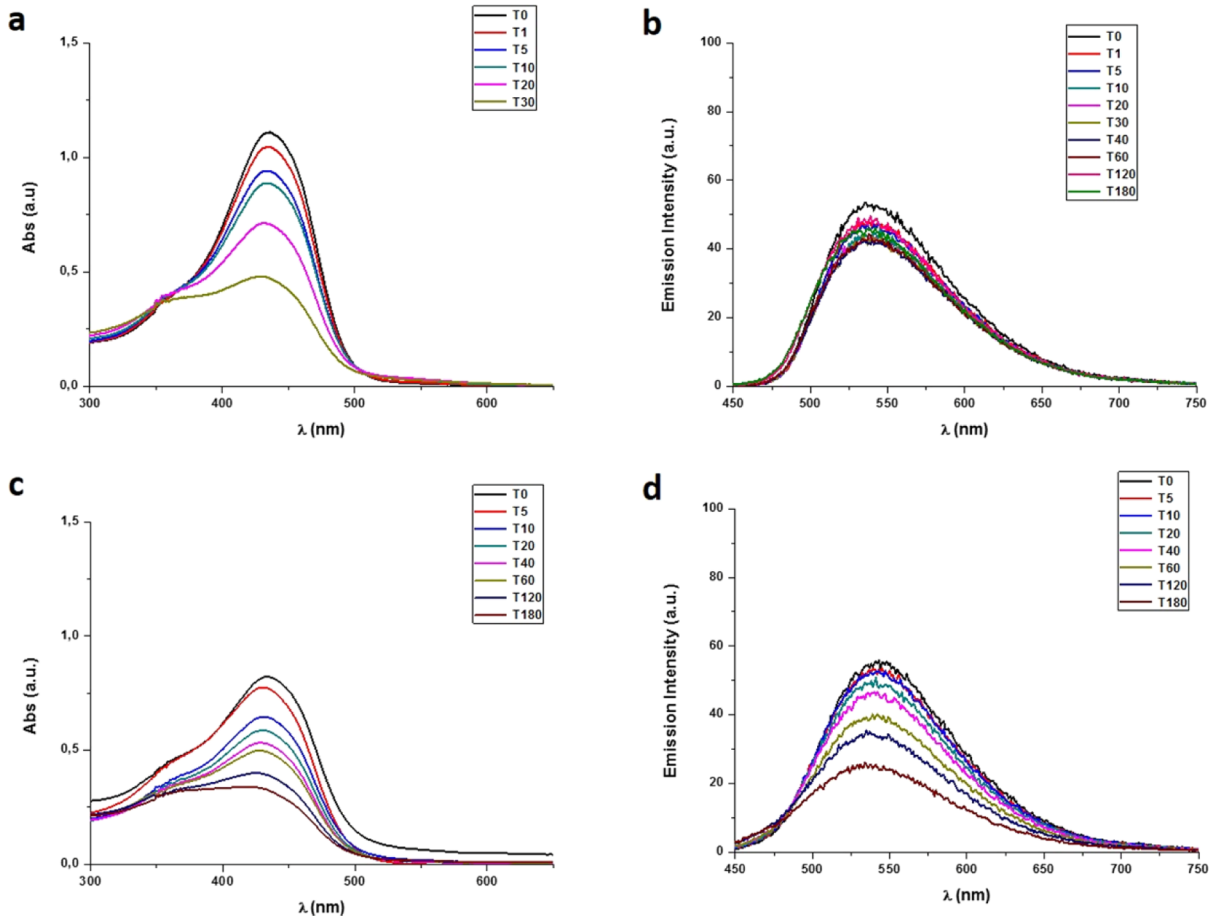

Figure 2. UV−vis spectra of cur (a) and Platicur NCs (c) in PBS (pH = 7.2). Emission spectra of cur (b) and Platicur NCs (d) in PBS (excitation wavelength = 430 nm).

In this method, the drug powder was added to a 0.1% chitosan solution prepared in diluted acetic acid. A series of experimental procedures were carried out in order to determine the polymer concentration and ultrasonication time. The process time was set to 20 min because beyond this time, the particle size does not further decrease. During sonication, the simultaneous deposition of a chitosan layer over the drug nanocore prevents aggregation and stabilizes the mixture, thanks to the strong positive charge of this polymer. After protocol optimization, nanocores with an external charge of about 31.7 ± 7.87 mV and 161.8 ± 1.3 nm (hydrodynamic diameter by DLS measurement, Figure S1) were obtained as reported in TEM and STEM images (Figure 1a,b). The whole-area TEM image is reported in the Supporting Information (Figure S2). NCs showed a rounded shape with an average diameter of about 100 nm ± 20.

Platicur NCs were further coated with different numbers of bilayers, consisting of chitosan and pectin, in order to obtain a multilayered nanoshell with different structural complexities. During the LbL process, the values of the zeta potential was measured after the deposition of each layer. The charge switches from the positive layer of chitosan to the negative layer of pectin. The values are always around ±25−30 mV. The colloidal stability is one of the main features of a nanoformulation because it is important to preserve the physicochemical properties. Stability studies of Platicur NCs coated with only chitosan or chitosan and pectin, $(CHI/PEC)_{2,5}$ and $(CHI/PEC)_{5,5}$, were performed over 2 weeks at room temperature, measuring the zeta potential and size every day, in order to establish the best conditions. Decreasing the number of bilayers, an improvement in colloidal stability occurred. The results are in accordance with the literature

https://dx.doi.org/10.1021/acsabm.0c00766
ACS Appl. Bio Mater. 2020, 3, 6836−6851

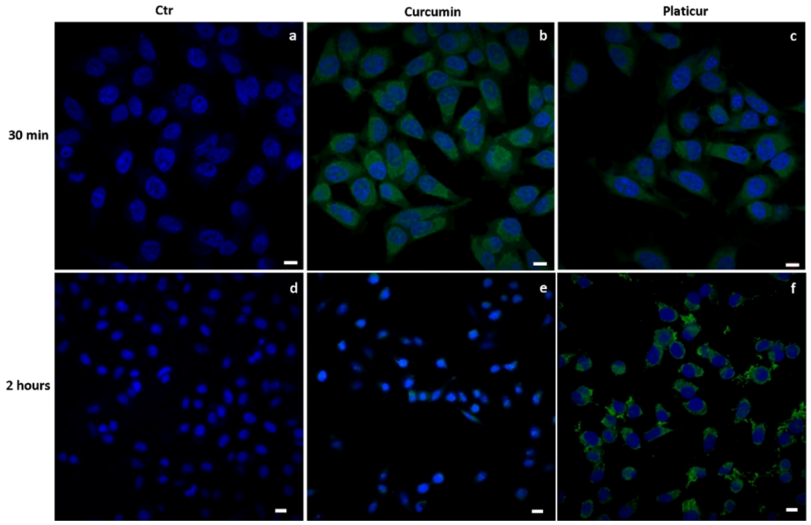

Figure 3. Confocal images of HeLa cells treated with 50 μM cur and 75 μM Platicur NCs in the dark for 30 min (top) and 2 h (bottom). Scale bar = 5 μm. (a) Control cells after 30 min; (b) cur-treated cells after 30 min; (c) Platicur-treated cells after 30 min; (d) control cells after 2 h; (e) cur-treated cells after 2 h; and (f) Platicur-treated cells after 2 h.

data.[29] Santos and co-worker, synthetizing the Ibuprofene nanocore, suggested that the colloidal stability is influenced by the number of bilayers. The worse conditions were obtained with drug nanoparticles coated with 7.5 bilayers of polyelectrolytes. Also, Parekh reported the same statement on nanoparticles containing camptothecin with a shell composed of eight polyelectrolyte bilayers.[41] Probably, a higher number of bilayers led to complexity of the system and the nanoparticles tends to aggregate.

The stability of Platicur NCs was also studied by spectroscopy measurements performed in PBS (phosphate-buffered saline, pH = 7.2), monitoring UV−vis and PL spectral changes with time. As reference, cur alone was used. The absorbance and the emission intensity were monitored for two weeks, storing the samples at 4 °C under dark conditions. The absorption spectra of Platicur NCs displayed a broad intense absorption band at 450 nm, like cur. The emission spectra were similar, showing a characteristic band at 530 nm (λ_{ex} = 430 nm). Platicur NCs had a slightly lower emission intensity, probably because of the presence of platinum (data not shown).

Under light irradiation, the absorption at 450 nm as a function of time reported a different behavior (Figure S3): cur at the beginning displayed an intense absorption at 450 nm but just after 30 min upon irradiation, it degraded rapidly; thus the peak intensity was halved. On the contrary, Platicur NCs maintained a high intensity of absorption even after 3 h of light irradiation. The UV−vis and PL spectra are reported in Figure 2. The samples were irradiated with visible light (400−700 nm, 2.5 J cm^{-2}) and the absorbance and fluorescence emission was recorded every 5 min for 3 h. The Platicur NC absorption spectra were slightly moved to the left (Figure 2c). The emission intensity of free cur and our nanoformulation was comparable.

These results indicate that the nanoformulation is stable in the darkness and the intensity remained unchanged; furthermore, the light is necessary for its activation.

In the literature,[42−44] similar complexes, although not in the nanoformulation form, showed different behaviors because under irradiation, the photodissociation of cur occurs. In fact, the photoexposure led to a gradual enhancement of emission intensity at 530 nm with a gradual decrement in absorbance, probably because of the detachment of cur.

Loading Efficiency and Release. Data analysis of quantitative measurements performed by ICP showed that the loading efficiency was around 85% for Platicur NCs. As reported in most of the controlled release delivery systems,[45] our nanoformulation exhibited an extended release profile of the cisplatin analogue from polymeric shells, depending on different numbers of adsorbed layers chitosan, $(CHI/PEC)_{2,5}$ and $(CHI/PEC)_{5,5}$. Controlled release is a desired characteristic for a carrier for cancer therapy. The kinetics of release is affected by the chemical structure and properties of the drug molecule associated with both the polymers and the drug. In the case of the polymeric shell, the drug could be released through the meshes of the polymer or after the polymer degradation. LbL technology, used in this work, allows the simple control of drug release rate by simple changes in coating thickness or composition. As shown in Figure S4, the release kinetic curves for cisplatin, with different coating thicknesses, under standard sink conditions, at the same drug concentration of 2 mg/mL decreased as the number of polyelectrolyte layers in the shell was increased, as expected.

Following the studies on colloidal stability and release kinetics, biological studies continued using the formulation Platicur NCs $(CHI/PEC)_{2.5}$.

BIOLOGICAL ACTIVITY

Confocal Microscopy. Confocal microscopy experiments were carried out in order to study the cellular localization of Platicur NCs. Exploiting cur fluorescence, it is possible to track NC localization inside cells without using other fluorescent probes. We imaged the cells after two time points of incubation with cur alone and Platicur NCs: 30 min and 2 h, because of fast degradation of cur. Figure 3 reports confocal micrographs: the nuclei of HeLa cells are stained blue and the fluorescence associated to cur is shown in green.

The NC internalization was very fast in HeLa cells: already after 30 min, it was possible to observe the green fluorescence in the cytoplasm (Figure 3c). Confocal analysis clearly confirmed that cur and NCs within 30 min efficiently and

https://dx.doi.org/10.1021/acsabm.0c00766
ACS Appl. Bio Mater. 2020, 3, 6836−6851

rapidly entered cells and showed their main localization in the cytoplasmic region. As already reported, cur degraded rapidly; indeed, no fluorescence appeared after 2 h of incubation in the darkness, Figure 3e, whereas in the case of Platicur NCs, the cur is firmly bonded to the platinum center, and an intense fluorescence was observed even after 2 h of incubation, Figure 3f.

Cell Viability Assay. In order to evaluate the anticancer effect of nanoformulation, an MTT assay[46] was performed. The experiments were carried out in the dark and under light conditions in a human cervical cancer cell line, namely, HeLa.

At first, an experiment of the dose−response curve was made in order to obtain the IC_{50} values of cur, cisplatin, and Platicur NCs in the darkness (data not shown) in HeLa cells. The estimated IC_{50} values are reported in Figure 4.

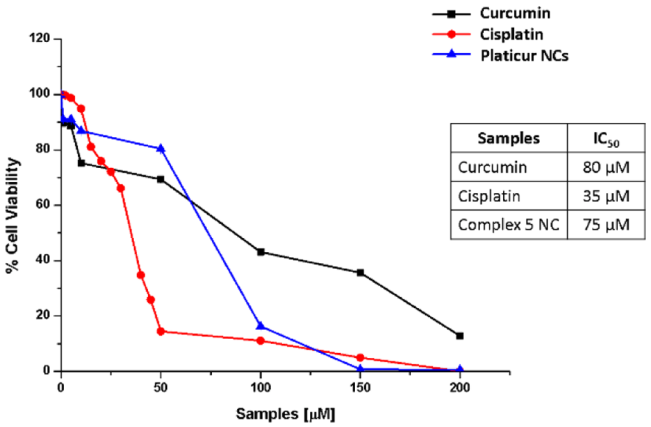

Figure 4. Dose−response curve and IC_{50} values of cur, cisplatin, and Platicur NCs obtained for HeLa cells.

Furthermore, an experiment aimed to test the synergic effect of cur and cisplatin was performed using the IC_{50} value of the metal-based anticancer drug and 10 μM cur, as reported in the literature.[47] A further reduction in cell viability was achieved up to 30%. All these obtained IC_{50} values were used in the photoexposure experiments. The experimental setup provides incubation of all samples for 4 h in the dark and then irradiation with visible light for 1 h (400−700 nm, 2.5 J cm^{-2}). An abrupt decrease in cell viability was observed in all samples containing cur; the only sample that was not affected by the photoexposure was that of cells treated with cisplatin. For this reason, we performed another MTT assay, testing the concentration of NCs (Figure 5) from 0.001 μM up to 1.0 μM, in order to evaluate the IC_{50} of Platicur NCs under photoirradiation. The results shown in Figure 5 demonstrated that the photoirradiation does not affect the cell health (black histogram). The results obtained with the NCs were very interesting, from the point of view of biological efficacy: the IC_{50} value found under irradiation was 0.05 μM (light gray histogram), a value 3 orders of magnitude lower than that under the conditions evaluated in the darkness. The results about the effect on cell viability after irradiation, observed in the literature for Pt complexes, suggested that our nanoformulation was more powerful because the decrease in cell viability reported in the literature was only about 1 order of magnitude. This data could be explained in terms of solubility, cellular uptake, and bioavailability. In fact, the nanotechnological approach offers multiple benefits associated with the biocompatibility, toxicity, good bioavailability, and solubility.

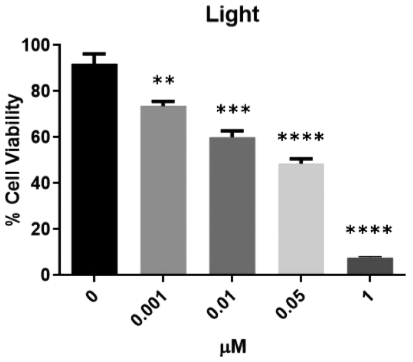

Figure 5. MTT assay in HeLa cell lines incubated with Platicur NCs for 4 h in the dark and then exposed to visible light for 1 h (400−700 nm, 2.5 J cm^{-2}). Values represent mean + SD and were obtained from three independent experiments. Statistically significant value $p < 0.01$ (**), very statistically significant $p < 0.001$ (***), and extremely statistically significant $p < 0.0001$ (****).

ROS Generation. 2′,7′-Dichlorofluorescein diacetate (DCFDA) assay was performed to study the generation of ROS in HeLa cells after incubation with the following samples: cur, cisplatin, cisplatin and cur, and Platicur NCs for 4 h. ROS play a significant role in signal transduction and cell metabolism. Thus, all samples were exposed to irradiation with visible light (400−700 nm) or kept in the darkness.[48] The concentration tested was the IC_{50} for all conditions as summarized in Table 1. In recent years, the literature reported

Table 1. IC_{50} Values of cur, Cisplatin, Cisplatin + cur, and Platicur NCs Tested in HeLa Cells

sample	IC_{50} (μM) DARK	IC_{50} (μM) LIGHT
cur	80	80
cisplatin	35	35
cisplatin + cur (combined treatment)	35 and 10 (respectively)	35 and 10 (respectively)
Platicur NCs	75	0.05

that the excessive amount of ROS production is closely related to the cytotoxicity induced by cisplatin treatment, which causes detrimental effects. In particular, ROS are involved in the apoptotic pathway; indeed, increased ROS generation alters the mitochondrial membrane, potentially damaging the respiratory chain.

cur cotreatment further enhances the effect of cisplatin. This increment in ROS production was probably due to the excessive influx of Ca^{2+}stimulated by cisplatin treatment in the mitochondria. cur affected the cell death by stimulation of ROS production through the activations of caspase, −3 and −9. After light irradiation, ROS stimulation is increased. Surprisingly, Platicur NCs lead to a decrease in ROS production. Probably, the mechanism induced by light irradiation led to a different activation of the apoptotic pathway, involving the phosphorylation of p53 tumor suppressor protein. This phenomenon has been already reported for cisplatin cotreatment with other antioxidant molecules, such as *N*-acetylcysteine, which is a precursor of glutathione (GSH) that can scavenge ROS to suppress its activity.[49]

In our experiment, the DCFDA-treated sample was used as the positive control. Under dark conditions, all treatments generate ROS between 45 and 80% in comparison with

https://dx.doi.org/10.1021/acsabm.0c00766
ACS Appl. Bio Mater. 2020, 3, 6836−6851

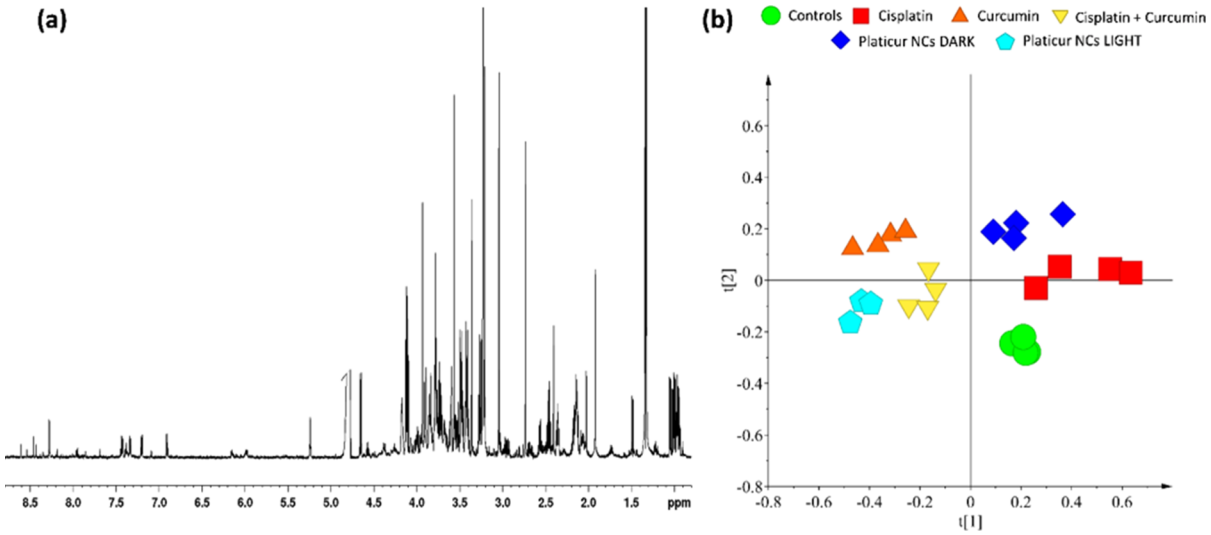

Figure 6. (a) Representative ^{1}H CPMG (Carr−Purcell−Meiboom−Gill) NMR spectrum of aqueous HeLa cell extracts. (b) PCA score plot of the ^{1}H NMR spectra (Pareto scaled) obtained from the aqueous extracts of treated HeLa cells. In detail, to make the ^{1}H NMR spectrum-derived data results comparable, the treatments with cisplatin, cur, cisplatin + cur, Platicur NC nonphotoactivated (DARK), and Platicur photoactivated (LIGHT) were set to the dose of IC_{50} and at the 24 h after treatment. The three-component PCA $t[1]/t[2]$ model gave R^2(cum) 0.774 and Q^2(cum) 0.657.

control, Figure S5. Under light irradiation, as expected, cur and cisplatin and cur caused a pronounced ROS production of around 90%. Surprisingly, cells treated with Platicur NCs showed the lowest ROS levels. The ROS production is inhibited by metabolic reprogramming of glucose metabolism (*e.g.*, when more NADPH is generated).[50]

METABOLOMICS STUDIES OF TREATED HELA CELLS AND CORRESPONDING CULTURE MEDIA: MULTIVARIATE ANALYSIS OF NMR DATA

Metabolic profiling of cultured cancer cells when exposed to drugs directly provides the information of cellular metabolic response to the environmental stimuli, thus offering valuable insights into drug mechanisms at the cellular level.[3,4,32,33] NMR spectroscopy is the major tool and detection technique in the metabolic change monitoring in terms of metabolites levels of expression induced by drug treatments.[3,4,33,35,51,52] NMR-based metabolomics is a new field in the anticancer research and only recently has been applied in the study of the metal-based drug mechanism of action.[3,4] Starting from the properties cited above about the Platicur NCs, we deemed it interesting to study in depth the NC Platicur photoactivation effects on cancer cells. Neither attempts of photoactivated nanoparticle study, without conjugated photosensitizers on the surface nor specific investigation about the metabolic alterations induced by photoactivated nanoparticles on cancer cell models has been previously reported. NMR metabolomics experiments were performed comparing the Platicur photoactivated NC (LIGHT) treatment with Platicur non-photoactivated NCs (DARK), cisplatin, cur and cisplatin (here indicated as cisplatin + cur), and cur on HeLa cells (human cervical cancer cell line). To better underline and highlight the metabolic differences induced by each treatment, the same experimental setup and design were used. Cell treatments were performed at the corresponding IC_{50} dose of each drug and the same sampling time of exposure (24 h). A total of 24 samples were examined.

^{1}H NMR spectra of HeLa cells (aqueous and lipid extracts) and corresponding culture media were acquired for all the considered conditions of treatment. The most statistically relevant changes between the different cell treatments were identified by a multivariate data analysis (MVA) of the acquired NMR spectral data. Unsupervised PCA and supervised OPLS-DA statistical analyses on the Pareto scaled[53] NMR data were performed. PCA analysis provides a general overview on the trends and patterns of data, simply describing the intrinsic variation in the spectral information and their potential clustering, depending on specific loadings. The further supervised method OPLS-DA focused on the discrimination effect of interest and needs a prior knowledge of sample clustering, so it was used in this work to examine the intrinsic variation in the data and for classification purposes.

The robustness and predictive capability (statistical model performance) were assessed through permutation tests (permutations = 100) and seven-fold cross-validation both to R^2 and Q^2 parameters to describe the total variations in the data and the predictability of models.

Aqueous HeLa Cell Extracts. ^{1}H NMR spectra of HeLa aqueous cell extracts, for each condition of treatment, were collected and primary resonances in the ^{1}H NMR spectra were assigned to individual metabolites and are reported in Table S1.

A preliminary PCA analysis was applied to the collected ^{1}H CPMG NMR data derived from the aqueous extracts of controls and all treated HeLa cells (Figure 6). A three-principal component model described more than 70% (R^2X = 0.774, Q^2 = 0.657) of the total variance, so reflecting a good robustness of group discrimination. It is possible to note that in the PCA model (Figure 6b), all treated samples clustered show a univocal metabolic behavior for each kind of treatment. PCA resulted in a clear separation along the $t[1]$ component (that describes the greatest data variance) between cur-, cisplatin + cur-, and Platicur NCs LIGHT-treated samples respect to cisplatin, Platicur NCs DARK, and untreated samples. Examination of the loadings (Figure S6) highlights that cur-,

https://dx.doi.org/10.1021/acsabm.0c00766
ACS Appl. Bio Mater. 2020, 3, 6836−6851

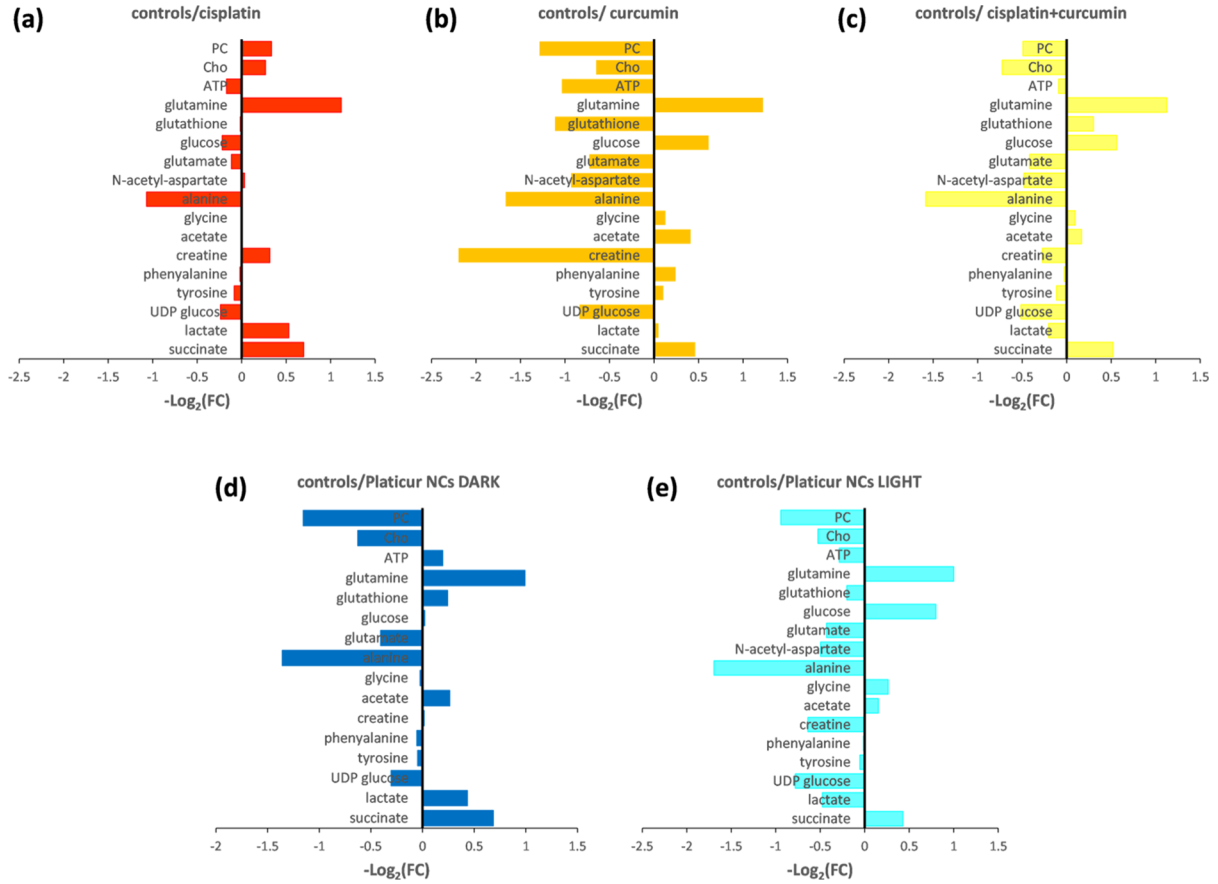

Figure 7. Relevant discriminant metabolite comparison of HeLa cell aqueous extracts obtained from different pairwise groups (different treatments compared to controls). For each metabolite, the statistical significance of the difference between the means of the pairwise groups was provided using the two-sample *t*-test. A *p*-value of < 0.05 (confidence level 95%) was considered for statistical variance. Metabolites with $-\text{Log}_2$ (FC) negative values have lower concentration in treated samples considered pairwise to controls (thus higher concentration in controls). Metabolites with $-\log_2$ (FC) positive values have higher concentration in treated samples considered pairwise to controls (thus lower concentration in controls). (a) Controls *vs* cisplatin; (b) controls *vs* cur; (c) controls *vs* cisplatin + cur; (d) controls *vs* Platicur NCs DARK; and (e) controls *vs* Platicur NCs LIGHT.

cisplatin + cur-, and Platicur NCs LIGHT-treated samples were characterized by a relatively high amount of glutamine, acetate, and glucose with respect to cisplatin, Platicur NCs DARK, and untreated samples which, in turn, were characterized by a relative higher amount of lactate, creatine, glycine, and choline derivatives [choline (Cho), phosphocholine (PC), and glycerophosphocholine (GPC)].

In order to improve the occurring class differences and to get insights into the metabolites responsible for class separation, further pairwise OPLS-DA models of treated samples with respect to controls were studied. Models were performed with the same number of predictive and orthogonal components (1 + 2 + 0), in order to better compare their quality parameters. OPLS-DA score plots, the corresponding S-line plots, and the robustness model parameters (R^2 and Q^2) are reported in Figure S7. The quality parameters clearly indicate a good possibility to differentiate pairwise each treated group sample from controls.

The spectral integration of the metabolites responsible for class separation in OPLS-DA models (previously identified and reported in Table S1) was carried out for signals that are clearly a representative of specific compounds and not affected by other overlapping signals. Pairwise comparison of the FC variation for the identified metabolites is reported in Figure 7.

The changes in metabolites with significant correlation coefficients, causing the different metabolic alterations in HeLa cells according to each treatment, are reported in Table S2. The analysis of the S-line plots, derived from OPLS-DA models (Figure S7), indicates that the metabolic-induced alterations are mainly due to different metabolites such as amino acids (alanine, glutamate, glycine, isoleucine, valine, glutamine, leucine, tyrosine, phenylalanine, histidine, and lysine), choline derivatives (Cho, PC, and GPC), acetate, succinate, lactate, *m*-inositol, taurine, creatine, GSH, *N*-acetylaspartate, glucose, UDP glucose, ATP, and formate.

In all treatments, we found higher relative levels of glutamine and succinate and lower levels of alanine and glutamate with respect to controls. Interestingly, the treatment with cur induced in HeLa cells significant modulations in metabolite expression 24 h after treatment. A marked decrease in GSH, alanine, ATP, and creatine levels was evidenced in cur treatment with respect to controls. Lactate was found higher only in cisplatin and Platicur NCs DARK treatments, whereas it is not discriminant in cur-treated samples with respect to controls. On the other hand, lactate was lower in both cisplatin + cur and Platicur NCs LIGHT compared to controls. Increase in lactate, the endproduct of anaerobic glycolysis (Warburg effect),[54,55] demonstrates a mismatch between glycolysis and oxygen supply.[55] Lower lactate levels observed in cisplatin +

https://dx.doi.org/10.1021/acsabm.0c00766
ACS Appl. Bio Mater. 2020, 3, 6836−6851

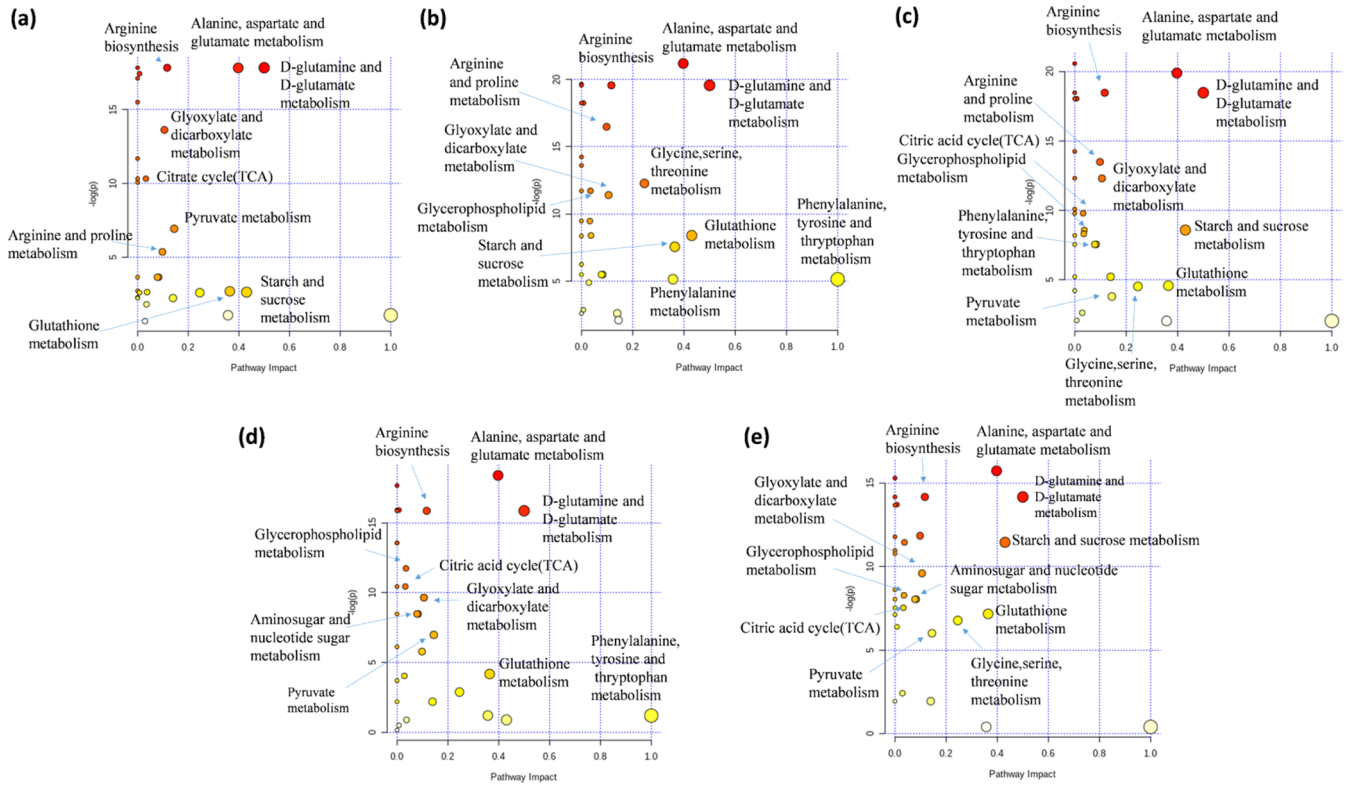

Figure 8. Summary of metabolic analysis conducted using MetaboAnalyst. (a) cisplatin *vs* controls; (b) cur *vs* controls; (c) cisplatin + cur *vs* controls; (d) Platicur NCs DARK *vs* controls; and (e) Platicur NCs LIGHT *vs* controls. Colors, varying from yellow to red, mean that the metabolites are in the data with different levels of significance (yellow: *p*-value < 0.1; light orange: *p*-value < 0.05; orange: *p*-value < 0.01; and red: *p*-value < 0.001). Circle size, varying from small to big, means the impact of metabolites in data on the pathways alteration (small circle—low impact and large circle—high impact).

cur and Platicur NCs LIGHT demonstrate a reduced conversion of pyruvate into lactate, a typical condition expressed in cancer cells during proliferation.[54,55]

Moreover, the NMR spectroscopy analysis of treated HeLa cells revealed low Cho and PC in the case of cur, cisplatin + cur, and Platicur NCs (both DARK and LIGHT), with respect to controls. On the contrary, cisplatin-treated HeLa cells showed higher expression of Cho and PC. It is well-known that Cho is a cell membrane condition marker and in most of the proliferative processes, an increased Cho level can be observed. The increase in the Cho level is considered as a sensitive index of phospholipid turnover caused by intensified proliferation of neoplastic cells, indirectly pointing to their accelerated growth.[56] The decreased levels of Cho found in cur-, cisplatin + cur-, and Platicur NC (both DARK and LIGHT)-treated samples, suggested that at 24 h after treatments, cells were metabolically inactive not maintaining the proliferation potential, typical of cancer cells.[57] Consistently, the monitoring of Cho decrease often is used as a control marker of response to therapy.[56,58] Cho contributes to the biosynthesis of phosphatidylcholine (PTC), the major component of a biological membrane.[59] Indeed, drug-induced apoptosis is generally accompanied by inhibition of the PTC biosynthesis, as revealed by the contemporary decrease in Cho and PC.[60] The here-observed contemporary decrease in Cho and PC for cur, cisplatin + cur, Platicur NC (both DARK and LIGHT) treatments could be explained by an earlier induction of apoptosis with respect to cisplatin. This latter is known to induce apoptosis at longer treatment times, resulting in Cho and PC levels still high after 24 h. The analysis of OPLS-DA models and related discriminant metabolites underlined a very similar metabolic stress response induced by cur, Platicur NCs LIGHT, and combined cisplatin + cur treatments. This suggests that the light activation of Platicur nanocolloids (Platicur NCs LIGHT), could induce the metal −O,O− donor ligand bond dissociation, therefore modulating the controlled release of cur, as noted in previous studies on Platicur.[13] Furthermore, an increase in lactate and GSH levels in Platicur NCs DARK and a decrease in Platicur NCs LIGHT treatments, with respect to the controls, were observed (Figures S7d,e and 7d,e). Low levels of GSH were observed only in the case of cur and Platicur NCs LIGHT treatment. The decrease in GSH expression suggests the presence of oxidative damage, as reported for other cancer cell drug treatment studies.[33] The two different metabolic profiles observed for light-activated or not activated Platicur NCs could be explained by the action of different compounds. In Platicur NCs LIGHT, dissociation may occur because of the light activation, probably originating from the aqua species of cisplatin and free cur. Consistently, the amount of glutamine, acetate, UDP-glucose, formate, lactate, succinate, creatine, glutamate, *N*-acetylaspartate, and alanine is very similar to that of cisplatin + cur treatment (Figure 7). In all treatments, except in Platicur NCs DARK, the decrease in ATP, with respect to controls, was also observed. The lowering of ATP levels is generally associated to a mitochondrial oxidative phosphorylation damage or to apoptotic processes. Indeed, although mitochondrial oxidative phosphorylation is an efficient ATP generating process, cells require a considerable amount of energy (ATP) to carry out the cellular

https://dx.doi.org/10.1021/acsabm.0c00766
ACS Appl. Bio Mater. 2020, 3, 6836−6851

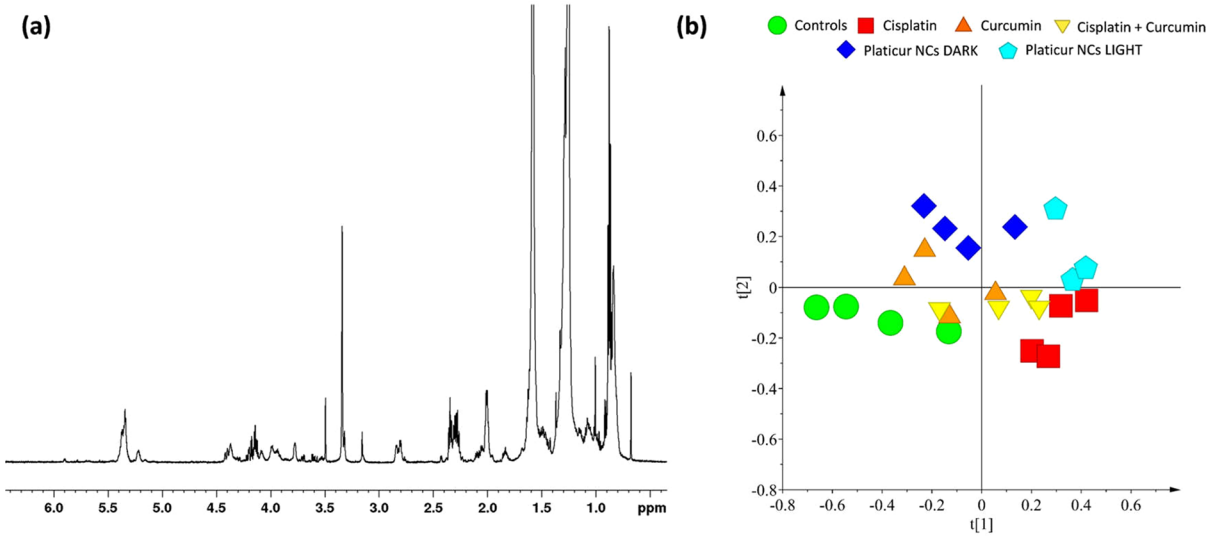

Figure 9. (a) ^{1}H zg NMR spectrum of lipidic HeLa cell extracts. (b) PCA score plot of the ^{1}H NMR spectra (Pareto scaled) obtained from the lipidic extracts of treated HeLa cells. In detail, to make the ^{1}H NMR spectrum-derived data results comparable, the treatments with cisplatin, cur, cisplatin + cur, Platicur NCs non-photoactivated (DARK), and Platicur photoactivated (LIGHT) were set up at the IC_{50} dose. The three-component PCA $t[1]/t[2]$ model gave R^2(cum) 0.928 and Q^2(cum) 0.794.

reorganization involved in programmed cell death during apoptosis.[52,61]

A peculiar metabolite involved in the stress-related metabolic variations that could be attributed to the presence of cur in the treatments is *N*-acetylaspartate (NAA). Interestingly, we found for cur, cisplatin + cur, Platicur NCs DARK, and Platicur NCs LIGHT a decrease in the *N*-acetylaspartate levels with respect to both controls and cisplatin treatments. NAA is one of the most highly upregulated metabolites in ovarian cancer. Selective *N*-acetylation of aspartate (a nonessential amino acid) is observed in ovarian cancers also characterized by increased NAA biosynthesis.[62] Moreover, Cancer Genome Atlas (TCGA, https://cancergenome.nih.gov/) reports worse clinical outcomes and survival for patients affected by ovarian, melanoma, renal cell, breast, colon, cervical, and uterine cancers, with elevated levels of NAA, thus proposing a general role for NAA as a specific cancer biomarker.[62] Interestingly, the limiting of NAA biosynthesis could prevent the tumor growth and increase patients' survival. It has been also reported that the targeting of the NAA pathway could have relevance for the development of future therapies for ovarian and other malignancies.[62]

Based on the observed quantitative variations for the identified metabolite content found in HeLa cells upon the different studied treatments, a metabolic pathway analysis using the MetaboAnalyst software[63] was performed. The most relevant pathways, potentially involved in the observed metabolic changes for treated HeLa cells (cisplatin, cur, cisplatin + cur, Platicur NCs DARK, and Platicur NCs LIGHT) according to the *p*-value and the impact value, are reported in Figure 8. The main potential target pathways altered in HeLa cells for each of the studied treatments included alanine, aspartate, and glutamate metabolism; D-glutamine and D-glutamate metabolism; arginine biosynthesis; and glyoxylate and dicarboxylate metabolism. Moreover, also the carbohydrate metabolism (starch and sucrose metabolism) appears to be compromised for all treated samples except in the case of Platicur NCs DARK treatment. The citric acid cycle and pyruvate metabolism resulted altered in all treatments with platinum compounds and not altered in the case of cur treatment alone. On the contrary, glycerophospholipid metabolism appears to be altered in all treatments in which is present cur (in the drug structure/formulation or alone) and not altered in the cisplatin treatment.

Lipidic HeLa Cell Extracts. Increasing attention has been recently focused on the lipid role in cells and in cancer and cancer treatment response studies;[3,64−66] this is mainly due to the significant alteration in lipid metabolism observed for this disease. For this reason, in order to extract maximum information from the studied treatments, the ^{1}H NMR spectroscopy and MVA of the spectral data were applied to the further investigation of the lipid cell fraction.

In this study, the NMR visible lipid spectrum of HeLa cell extracts in $CDCl_3$ (Figure 9a) consists of a number of signals, that are reported in Table S3. The dominant resonances arise from protons on the fatty acyl chains, especially from methylene $(-CH_2-)_n$ of fatty acyl chain length and methyl (CH_3-) groups at 1.28 and 0.88 ppm, respectively. Other resonances arise from protons of the vinylic ($-CH{=}CH-$ at 5.35 ppm), bis allylic ($=CH-CH_2-CH=$ at 2.8 ppm), and mono allylic ($CH_2-CH{=}CH-$ at 1.96−2.15 ppm) moiety of mono- and polyunsaturated lipids. An additional group of resonances is assigned to protons in the alpha ($-OOC-CH_2-CH_2-$ at 2.24−2.44 ppm) and beta ($-OOC-CH_2-CH_2-$ at 1.63 ppm) position of the carboxyl head group of the fatty acids (f.a.). Further resonances are from the lysophosphatydilcholine (LPTC) and phosphatydilcholine (PTC) head groups ($N^+(CH_3)_3$ at 3.32 and 3.34 ppm, respectively) and from the glycerol backbone of triglycerides (TG) (1,3-CH_2 at 4.1−4.3 ppm and 2-CH_2 at 5.31 ppm) and from the backbone of total glycerophospholipids (3-CH_2 at 3.97 ppm and 2-CH at 5.22), except LPTC.

A preliminary PCA analysis was carried out using the collected ^{1}H zg NMR data of the lipid extracts for controls and drug-treated HeLa cells (Figure 9b). A three-principal component model described more than 90% (R^2X = 0.928, Q^2 = 0.794) of total variance, reflecting the good robustness of

https://dx.doi.org/10.1021/acsabm.0c00766
ACS Appl. Bio Mater. 2020, 3, 6836−6851

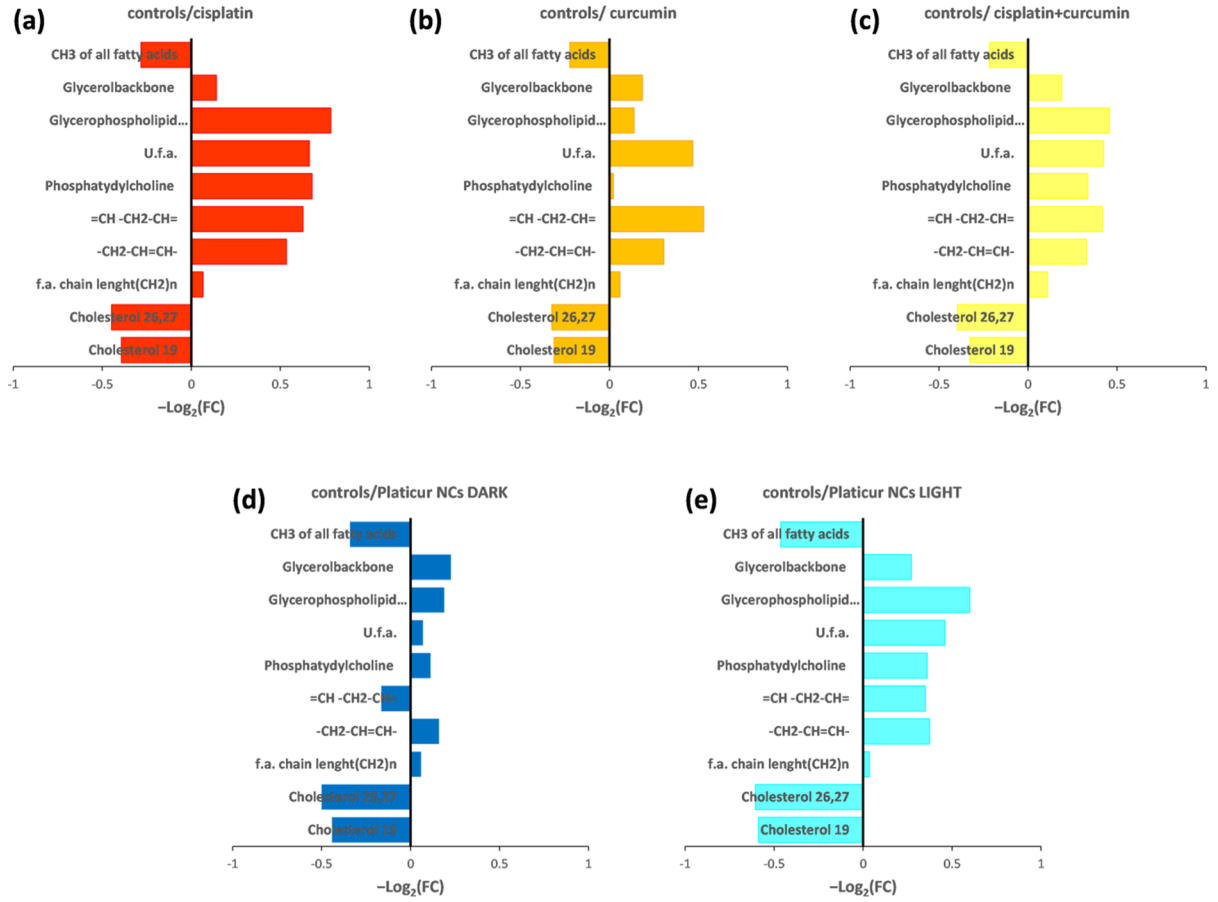

Figure 10. Relevant discriminant metabolite comparison of HeLa cell lipidic extracts obtained from different pairwise groups (different treatments compared to controls). For each selected lipid-related signal, the statistical significance of the difference between the means of the pairwise groups was provided using the two-sample *t*-test. A *p*-value of < 0.05 (confidence level 95%) was considered for statistical variance. Metabolites with $-\log_2$ (FC) negative values have lower concentration in treated samples considered pairwise to controls (thus higher concentration in controls). Metabolites with $-\mathrm{Log}_2$ (FC) positive values have higher concentration in treated samples considered pairwise to controls (thus lower concentration in controls). (a) Controls *vs* cisplatin; (b) controls *vs* cur; (c) controls *vs* cisplatin + cur; (d) controls *vs* Platicur NCs DARK; and (e) controls *vs* Platicur NCs LIGHT.

the model. In the PCA of lipid extracts, the separation among the six different treatment conditions is less-pronounced, with respect to the aqueous extracts. However, the PCA resulted in a small separation for all the treatments along the $t[1]$ component with controls at lowest $t[1]$ values and cisplatin together with Platicur NCs LIGHT at highest $t[1]$ values. The examination of loadings (Figure S8) highlights that cisplatin and Platicur NCs LIGHT-treated samples were characterized by a relatively higher amount of PTC, polyunsaturated fatty acids (p.u.f.a), and TG with respect to controls which, in turn, were characterized by a higher level of cholesterol.

With the same approach used for aqueous extracts, further supervised OPLS-DA pairwise analyses comparing treated samples and controls were carried out. Models with the same number of predictive and orthogonal components (1 + 2 + 0) were built, in order to better compare their quality parameters. The latter clearly indicated a good possibility to differentiate pairwise each of the treated group samples from the controls. OPLS-DA score plots and corresponding S-line plots are reported in Figure S9. The spectral integration of previously identified lipid resonances (Table S3), responsible for class separation in OPLS-DA models, was carried out. The calculated FC ratio ($-\mathrm{Log}_2$) of the normalized median intensity for each treatment with respect to the controls, considering the distinctive lipid signals in the spectra, is reported in Figure 10.

The inspection of the pairwise OPLS-DA models for the different treatments at 24 h, with respect to controls, revealed the lipid signals responsible for the observed class separations (Figure S9). In particular, it is possible to observe a similar variation in the general lipid content for the treatments with cisplatin, Platicur NCs LIGHT, and cisplatin + cur when compared to controls. The variation consists of marked lowering in cholesterol and rising in TG, unsaturated f.a., glycerophospholipids, and PTC levels, with respect to untreated cells. The same lipid profile alteration also occurs in the cur treatment despite the PTC content remains strictly comparable to that of controls. On the other hand, in Platicur NCs DARK treatment, only a weak increase in TG, unsaturated f.a., glycerophospholipids, and PTC content was observed, with respect to controls. However, a marked decrease in cholesterol and f.a. (such as observed for the other treatments) and a weak decrease in p.u.f.a. resulted from the FC analysis also for NCs DARK treatment.

As reported, highly proliferative cancer cells show a strong lipid and cholesterol avidity and therefore are generally characterized by an increase in their endogenous synthesis (lipogenesis and cholesterol synthesis, respectively).[64] Con-

https://dx.doi.org/10.1021/acsabm.0c00766
ACS Appl. Bio Mater. 2020, 3, 6836−6851

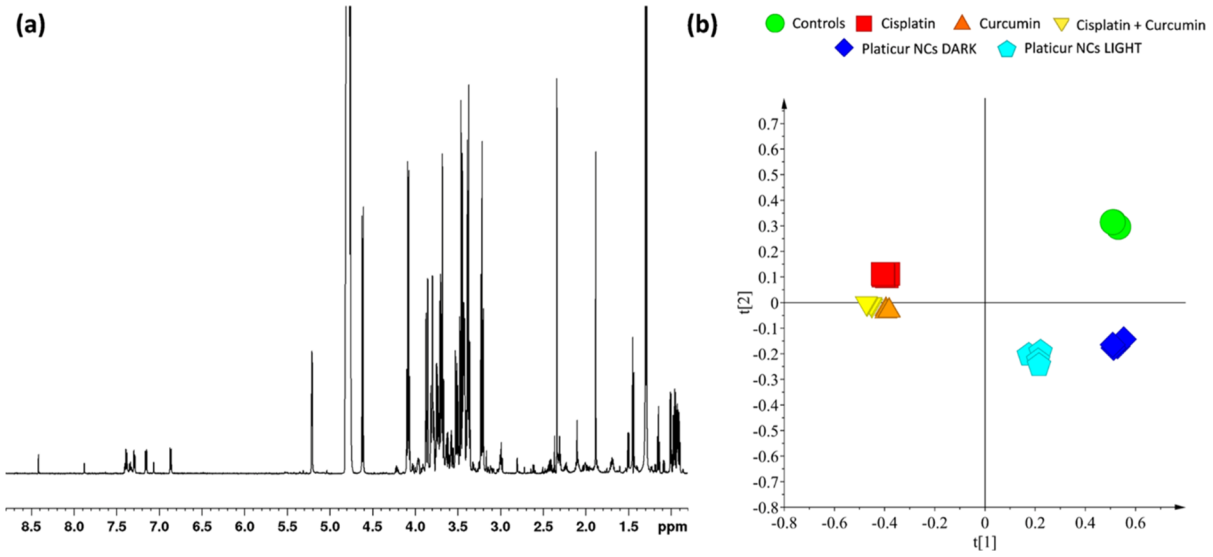

Figure 11. (a) Representative ^{1}H CPMG (Carr−Purcell−Meiboom−Gill) NMR spectrum of the HeLa cell culture media. (b) PCA score plot of the ^{1}H cpmg NMR spectra (Pareto scaled) obtained from the culture media of treated HeLa cells. In detail, to make the ^{1}H NMR spectrum-derived data results comparable, the treatments with cisplatin, cur, cisplatin + cur, Platicur NCs non-photoactivated (DARK), and Platicur photoactivated (LIGHT) were set to the dose of IC_{50} and at the 24 h after each treatment. The two-component PCA $t[1]/t[2]$ model gave R^2(cum) 0.949 and Q^2(cum) 0.934.

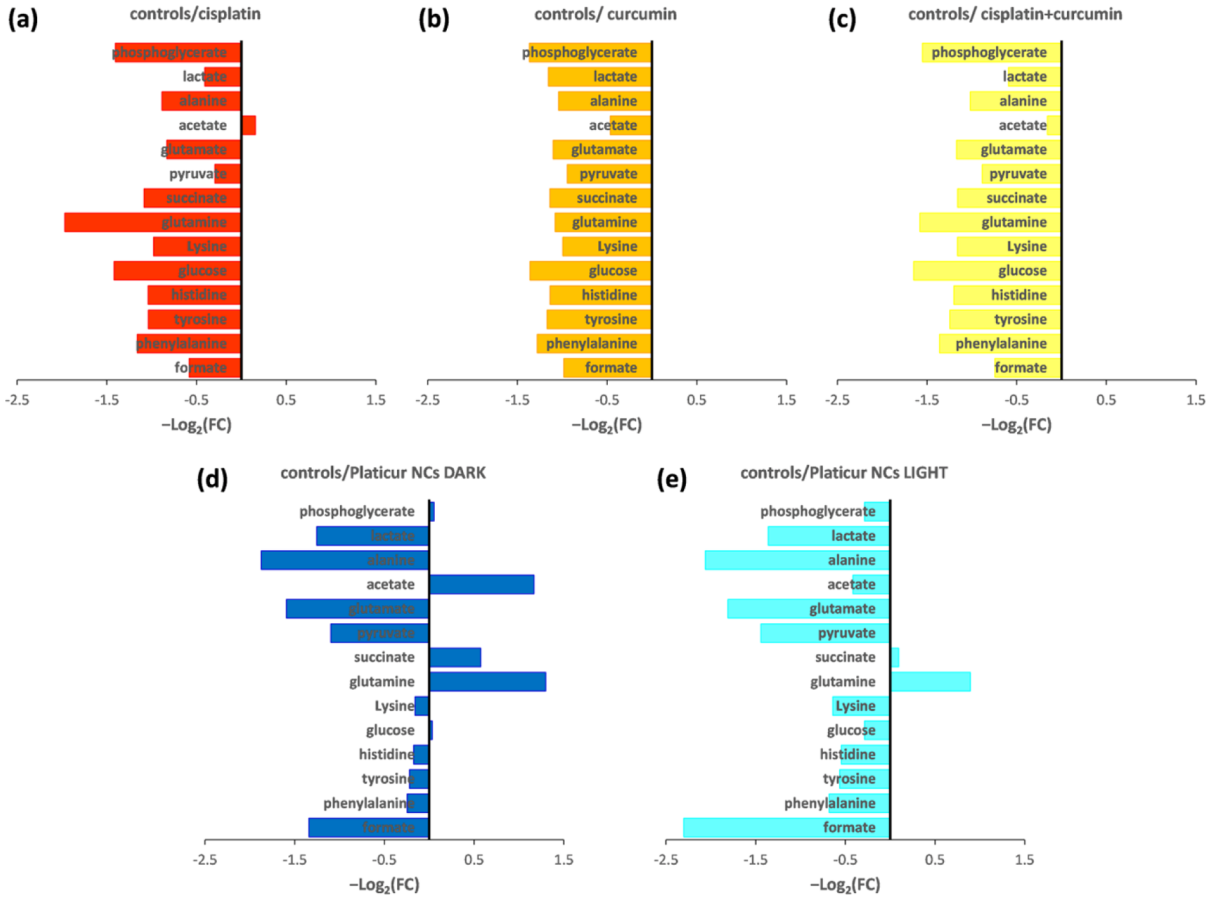

Figure 12. Relevant discriminant metabolite comparison of the HeLa cell culture media obtained from different pairwise groups (different treatments compared to controls). For each selected metabolite, the statistical significance of the difference between the means of the pairwise groups was provided using the two-sample *t*-test. A *p*-value of < 0.05 (confidence level 95%) was considered for statistical variance. Metabolites with $-Log_2$ (FC) negative values have lower concentration in treated samples considered pairwise to controls (thus higher concentration in controls). Metabolites with $-Log_2$ (FC) positive values have higher concentration in treated samples considered pairwise to controls (thus lower concentration in controls). (a) Controls *vs* cisplatin; (b) controls *vs* cur; (c) controls *vs* cisplatin + cur; (d) controls *vs* Platicur NCs DARK; and (e) controls *vs* Platicur NCs LIGHT.

https://dx.doi.org/10.1021/acsabm.0c00766
ACS Appl. Bio Mater. 2020, 3, 6836−6851

sistently, the OPLS-DA pairwise analysis showed high levels of cholesterol in active proliferating cells (controls) compared to treated cells (at the respective IC_{50} doses) where the drug stress is inducing cell death. On the contrary, in treated cells, an increase in the average aliphatic chain length, unsaturation degree, glycerophospholipids, and TG was found. In several types of tumor cells, the enhancement of these lipids has been consistently noted and correlated to cells undergoing apoptosis.[3,33,65,66] It is interesting to note, in the present case, that the general lipid content of Platicur NCs LIGHT-treated cells appears superimposable to that of cisplatin + cur treatment. This is in agreement with the aqueous extract analysis results and confirms the hypothesis of the light-induced Platicur cleavage, also when incorporated in NCs. The suggested cisplatin release (as aquospecies) from Platicur is strongly supported by the consequent triggering of apoptosis, indicated by lipid profile analysis, in accord with the literature data.[33,42,43]

Compositional Changes of Culture Media due to Treatments. The alteration in metabolite composition of cell culture media, upon drug exposure, allows detection of the utilization and/or release of specific substances, giving useful information about the physiological status of studied cell cultures.[3,52] ^{1}H NMR spectra of HeLa cell culture media (Figure 11a) for each treatment, after 24 h, were collected and primary resonances in the ^{1}H NMR spectra were assigned to individual metabolites and are reported in Table S1. Nutrient substrates, such as amino acids (isoleucine, valine, leucine, tyrosine, histidine, lysine, glutamine, phenylalanine, alanine, glycine, and glutamate) and glucose, the essential elements for cell growth, characterize the culture medium NMR spectra. Moreover, metabolites such as intermediates of the glycolysis and TCA cycle (phosphoglycerate, pyruvate, succinate, acetate, and lactate), carboxylic acids (isobutyrate), and waste metabolites (formate) were found. In the MVA of ^{1}H-CPMG-NMR spectra, the PCA model (2 components) explained 94.9% of the total variance (R^2(cum) 0.949 and Q^2(cum) 0.934). A clear discrimination was observed along the $t[1]$ component for the culture medium composition of cisplatin-, cur-, and cisplatin + cur-treated HeLa cells, with respect to controls, Platicur NCs DARK and Platicur NCs LIGHT, Figure 11b. Loading analysis (Figure S10) highlights that controls, Platicur NCs DARK- and Platicur NCs LIGHT-treated samples, are characterized by a higher amount of lactate, alanine, glucose, glycine, isoleucine, valine, leucine, and glutamine with respect to cisplatin-, cur-, and cisplatin + cur-treated cells.

A further supervised OPLS-DA analysis of the collected NMR data was carried out to optimize the observed class differences and obtain detailed information about nutrient consumption and metabolic endproducts released in the cell culture media. Each treatment was therefore compared pairwise with the controls, using NMR data. Again, to compare better their quality parameters, models have been built with the same number of predictive and orthogonal components (1 + 2 + 0). OPLS-DA score plots and corresponding S-line plots are reported in Figure S11. The quality model parameters indicate a good possibility to differentiate pairwise each culture media of treated groups from controls, as also observed by the clear separation along the $t[1]$ predictive component of the OPLS-DA models. Whenever possible, previously identified metabolites (Table S1), responsible for class separation, were integrated. The FC ratio of the normalized median intensity for each treatment with respect to the controls, considering the distinctive metabolites in the spectra, is reported in Figure 12.

The NMR profile of treated HeLa cell culture media and the OPLS-DA analysis demonstrated expected metabolic differences between treated and untreated cells. The consuming of the nutrients such as glucose and several amino acids and the producing of metabolic endproducts such as pyruvate, lactate, succinate, formate, phosphoglycerate, and acetate resulted from the analysis of culture media, following each considered treatment, in comparison with controls. Both OPLS-DA and FC analyses showed a similar metabolic trend for cisplatin, cur, and cisplatin + cur (Figures S11a–c and 12 a–c) treatments. In particular, lowering of all metabolite levels present in the media (both amino acids and cellular metabolic intermediates) was observed with respect to controls. The only observed difference, among these three treatments, consists of the increase in acetate found in the culture media of cisplatin-treated cells, respect to controls. This increase contrasts the generally observed decrease in cur- and cisplatin + cur-treated cells when compared to controls. Further metabolic changes were observed from the OPLS-DA models of Platicur NCs DARK and LIGHT culture media in comparison with controls. Higher levels of glutamine and succinate were observed. Moreover, the culture medium of Platicur NCs DARK was characterized by a generally higher content of acetate with respect to controls, only found also in cisplatin treatment. Platicur NCs DARK and LIGHT culture media also showed, as the other treatments (cisplatin, cur, and cisplatin + cur), a decrease in lactate, alanine, glutamate, pyruvate, alanine, isoleucine, valine, leucine, glycine, histidine, phenylalanine, tyrosine, and formate.

Cancer cells are frequently characterized by the tendency to convert pyruvate into lactate, known as the "Warburg effect".[55] Consistently, in controls, with respect to treated samples, higher levels of lactate and pyruvate were found in the culture media, as a result of an active glycolytic process in proliferating cancer cells. In this study, all treated cells showed lower levels of alanine, lactate, and pyruvate in the culture media, compared to controls (Figures S11 and 12). Alanine is released as a energy source from the alanine–glucose cycle after the formation of pyruvate from glycolysis.[52] The lower levels of lactate indicate a lower conversion of pyruvate into lactate. Moreover, the lower levels of both alanine and pyruvate suggest that the low production of lactate may be a consequence of the pyruvate synthesis inhibition. Glutamine is very important to maintain Krebs cycle efficiency in cancer cells.[67] Higher levels of glutamine in culture media found in Platicur NCs (LIGHT and DARK) indicate the reduced utilization of glutamine, a condition often associated to cell death.[67] The analysis of culture media after 24 h suggests that the stress response of cells under drug exposure results in high energy and glucose supply variations. In summary, at the same time of drug exposure, HeLa cells show selective consumptions of nutrients in response to growth needs and according to the different drug exposures, thus indicating different cellular responses and different adaptive mechanisms.

CONCLUSIONS

In this work, chitosan–pectin polysaccharides were chosen as Platicur delivery systems obtaining Platicur nanocolloids of about 100 nm, by ultrasonication-assisted LbL. Studies of different formulations of Platicur nanocolloids have been performed and the $(CHI/PE)_{2,5}$ formulation appeared to be

https://dx.doi.org/10.1021/acsabm.0c00766
ACS Appl. Bio Mater. 2020, 3, 6836–6851

the best in terms of controlled release and enhanced bioavailability. Moreover, the light-activated Platicur NCs showed an IC_{50} value (IC_{50} 50 nM) 3 orders of magnitude lower than that of Platicur NCs in the darkness (IC_{50} 75 μM), as stemmed by *in vitro* cytotoxicity evaluation.

A ^{1}H NMR metabolomics approach was used to detect in depth the metabolic profile of the HeLa cancer cell line (cervix cancer cell line) treated with light-activated Platicur NCs. This study compared the metabolic alterations induced by Platicur NCs LIGHT and DARK with those of cisplatin, cur, and cisplatin + cur (as coadministered drugs) on HeLa cells. The NMR−metabolomics analysis results unveiled that the light-activated Platicur NCs induced metabolic alterations that are strictly comparable to those of the combined treatment cisplatin + cur (characterized by a higher IC_{50} and low solubility because of the presence of cur). The hypothesis that the photoactivation of Platicur NCs induces cur and cisplatin aqua species release is strongly supported by the metabolomics investigation. Furthermore, observed metabolic alterations due to Platicur NCs LIGHT treatment are typically attributed to apoptotic phenomena. These include the decrease in Cho and PC (in aqueous extracts) and the increase in the PTC, unsaturation degree, and TG levels (in lipidic extracts) found in HeLa cells treated with Platicur NCs LIGHT. Based on these results, it can be concluded that Platicur NCs LIGHT induce cellular metabolic stress response because of a combined synergistic effect of cisplatin and cur. The use of Platicur NCs and their stability under physiological conditions could allow a controlled drug release. Moreover, the nontoxicity in the darkness and the very low IC_{50} are very interesting properties for possible side-effect reductions, therefore promoting Platicur NCs as very attractive photochemotherapeutic drug.

■ ASSOCIATED CONTENT

Supporting Information

The Supporting Information is available free of charge at https://pubs.acs.org/doi/10.1021/acsabm.0c00766.

Scheme of Platicur photolysis; size distribution of Platicur NCs obtained by DLS measurement; TEM characterization of Platicur NCs; absorbance at 450 nm *vs* time; controlled cisplatin release profiles; ROS production; PCA loading plot of the aqueous extracts of treated HeLa cells; chemical shifts (δ) and assignments of metabolite resonances in the ^{1}H NMR spectrum of Hela cells aqueous extracts; overview of metabolite variations between treatments; OPLS-DA score plots and S-line plots of HeLa cells aqueous extracts obtained from different pairwise groups; PCA loading plot of the lipid extracts of treated HeLa cells; chemical shifts (δ) and assignments of metabolite resonances in the ^{1}H NMR spectrum of HeLa cells lipidic extracts; OPLS-DA score plots and S-line plots of HeLa cells lipidic extracts obtained from different pairwise groups; PCA loading plot of the culture media of treated HeLa cells; OPLS-DA score plots and S-line plots of HeLa cell culture media obtained from different pairwise groups (PDF)

■ AUTHOR INFORMATION

Corresponding Authors

Viviana Vergaro − *Department of Biological and Environmental Sciences and Technologies (DiSTeBA), University of Salento, 73100 Lecce, Italy; Institute of Nanotechnology, CNR NANOTEC, Consiglio Nazionale delle Ricerche, 73100 Lecce, Italy*; Email: Viviana.vergaro@unisalento.it

Francesco Paolo Fanizzi − *Department of Biological and Environmental Sciences and Technologies (DiSTeBA), University of Salento, 73100 Lecce, Italy*; orcid.org/0000-0003-3073-5772; Email: Fp.fanizzi@unisalento.it

Giuseppe Ciccarella − *Department of Biological and Environmental Sciences and Technologies (DiSTeBA), University of Salento, 73100 Lecce, Italy; Institute of Nanotechnology, CNR NANOTEC, Consiglio Nazionale delle Ricerche, 73100 Lecce, Italy*; Email: Giuseppe.ciccarella@unisalento.it

Authors

Federica De Castro − *Department of Biological and Environmental Sciences and Technologies (DiSTeBA), University of Salento, 73100 Lecce, Italy*

Michele Benedetti − *Department of Biological and Environmental Sciences and Technologies (DiSTeBA), University of Salento, 73100 Lecce, Italy*

Francesca Baldassarre − *Department of Biological and Environmental Sciences and Technologies (DiSTeBA), University of Salento, 73100 Lecce, Italy; Institute of Nanotechnology, CNR NANOTEC, Consiglio Nazionale delle Ricerche, 73100 Lecce, Italy*

Laura Del Coco − *Department of Biological and Environmental Sciences and Technologies (DiSTeBA), University of Salento, 73100 Lecce, Italy*

Maria Michela Dell'Anna − *DICATECh, Politecnico di Bari, 70125 Bari, Italy*

Piero Mastrorilli − *DICATECh, Politecnico di Bari, 70125 Bari, Italy*; orcid.org/0000-0001-8841-458X

Complete contact information is available at: https://pubs.acs.org/10.1021/acsabm.0c00766

Author Contributions

V.V., G.C., and F.P.F. designed experiments and interpreted data; V.V. carried out the synthesis of nanocolloids and all biological experiments; F.D.C. carried out all metabolomics investigations; F.B. carried out TEM characterization; M.B., L.D.C., M.M.D.A., and P.M. provided critical input to the overall research direction; and F.D.C. and V.V. wrote the manuscript with input from all co-authors.

Funding

This study was supported by "Tecnopolo di Nanotecnologia e Fotonica per la Medicina di Precisione" (TECNOMED)-FISR/MIUR-CNR: delibera CIPE n.3449 del 7/08/2017, CUP: B83B17000010001; "Tecnopolo per la Medicina di precisione" (TecnoMed Puglia) - Regione Puglia: DGR n.2117 del 21/11/2018, CUP: B84I18000540002; Italian Ministero dell'Istruzione, dell'Universita' e della Ricerca within the program: Assegnazione risorse ai Consorzi Interuniversitari di Ricerca per "Progetti competitivi" (Decreto Ministeriale 29 marzo 2016 n. 202); and the PON 254/Ric. Potenziamento del "CENTRO RICERCHE PER LA SALUTE DELL'UOMO E DELL'AMBIENTE" Cod. PONa3_00334.

https://dx.doi.org/10.1021/acsabm.0c00766
ACS Appl. Bio Mater. 2020, 3, 6836−6851

Notes

The authors declare no competing financial interest.

■ ACKNOWLEDGMENTS

The University of Salento (Italy) and the Consorzio Interuniversitario di Ricerca in Chimica dei Metalli nei Sistemi Biologici (CIRCMSB), Bari (Italy) are acknowledged.

■ ABBREVIATIONS

NCs, nanocolloids; cur, curcumin; Platicur NCs LIGHT, photoactivated Platicur nanocolloids; Platicur NCs DARK, non photoactivated Platicur nanocolloids; PCA, principal component analysis; OPLS-DA, orthogonal partial least square discriminant analysis; Cho, choline; PC, phosphocholine; GPC, glycerophosphocholine; PTC, phosphatidylcholine; TG, triglycerides; f.a., fatty acids; FACS, fluorescence activated cell sorter; ROS, reactive oxygen species

■ REFERENCES

(1) Benedetti, M.; De Castro, F.; Romano, A.; Migoni, D.; Piccinni, B.; Verri, T.; Lelli, M.; Roveri, N.; Fanizzi, F. P. Adsorption of the cis-$[Pt(NH_3)_2(P_2O_7)]^{2-}$ (phosphaplatin) on hydroxyapatite nanocrystals as a smart way to selectively release activated cis-$[Pt(NH_3)_2Cl_2]$ (cisplatin) in tumor tissues. *J. Inorg. Biochem.* **2016**, *157*, 73−79.

(2) Benedetti, M.; Romano, A.; De Castro, F.; Girelli, C. R.; Antonucci, D.; Migoni, D.; Verri, T.; Fanizzi, F. P. N7-platinated ribonucleotides are not incorporated by RNA polymerases. New perspectives for a rational design of platinum antitumor drugs. *J. Inorg. Biochem.* **2016**, *163*, 143−146.

(3) De Castro, F.; Benedetti, M.; Antonaci, G.; Del Coco, L.; De Pascali, S.; Muscella, A.; Marsigliante, S.; Fanizzi, F. Response of Cisplatin Resistant Skov-3 Cells to [Pt(O,O′-Acac)(γ-Acac)(DMS)] Treatment Revealed by a Metabolomic ^{1}H-NMR Study. *Molecules* **2018**, *23*, 2301.

(4) De Castro, F.; Benedetti, M.; Del Coco, L.; Fanizzi, F. P. NMR-Based Metabolomics in Metal-Based Drug Research. *Molecules* **2019**, *24*, 2240.

(5) Mandriota, G.; Di Corato, R.; Benedetti, M.; De Castro, F.; Fanizzi, F. P.; Rinaldi, R. Design and Application of Cisplatin-Loaded Magnetic Nanoparticle Clusters for Smart Chemotherapy. *ACS Appl. Mater. Interfaces* **2019**, *11*, 1864−1875.

(6) Gupta, S.; Pathak, Y.; Gupta, M. K.; Vyas, S. P. Nanoscale drug delivery strategies for therapy of ovarian cancer: conventional vs targeted. *Artif. Cells, Nanomed., Biotechnol.* **2019**, *47*, 4066−4088.

(7) Li, J.; Cai, C.; Li, J.; Li, J.; Li, J.; Sun, T.; Wang, L.; Wu, H.; Yu, G. Chitosan-Based Nanomaterials for Drug Delivery. *Molecules* **2018**, *23* (), DOI: DOI: 10.3390/molecules23102661.

(8) Bednarski, P.; Fiona, S. M.; Peter, J. S. Photoactivatable Platinum Complexes. *Anti-Cancer Agents Med. Chem.* **2007**, *7*, 75−93.

(9) Farrer, N. J.; Salassa, L.; Sadler, P. J. Photoactivated chemotherapy (PACT): the potential of excited-state d-block metals in medicine. *Dalton Trans.* **2009**, 10690−10701.

(10) Mackay, F. S.; Woods, J. A.; Heringová, P.; Kašpárková, J.; Pizarro, A. M.; Moggach, S. A.; Parsons, S.; Brabec, V.; Sadler, P. J. A potent cytotoxic photoactivated platinum complex. *Proc. Natl. Acad. Sci. U.S.A.* **2007**, *104*, 20743−20748.

(11) Chifotides, H. T.; Dunbar, K. R. Interactions of Metal−Metal-Bonded Antitumor Active Complexes with DNA Fragments and DNA. *Acc. Chem. Res.* **2005**, *38*, 146−156.

(12) Farrer, N. J.; Woods, J. A.; Salassa, L.; Zhao, Y.; Robinson, K. S.; Clarkson, G.; Mackay, F. S.; Sadler, P. J. A Potent Trans-Diimine Platinum Anticancer Complex Photoactivated by Visible Light. *Angew. Chem.* **2010**, *122*, 9089−9092.

(13) Mitra, K.; Gautam, S.; Kondaiah, P.; Chakravarty, A. R. The cis-Diammineplatinum(II) Complex of Curcumin: A Dual Action DNA Crosslinking and Photochemotherapeutic Agent. *Angew. Chem., Int. Ed. Engl.* **2015**, *54*, 13989−13993.

(14) Panda, A. K.; Chakraborty, D.; Sarkar, I.; Khan, T.; Sa, G. New insights into therapeutic activity and anticancer properties of curcumin. *J. Exp. Pharmacol.* **2017**, *9*, 31−45.

(15) Calixto, G.; Bernegossi, J.; de Freitas, L.; Fontana, C.; Chorilli, M. Nanotechnology-Based Drug Delivery Systems for Photodynamic Therapy of Cancer: A Review. *Molecules* **2016**, *21*, 342.

(16) Banerjee, S.; Chakravarty, A. R. Metal Complexes of Curcumin for Cellular Imaging, Targeting, and Photoinduced Anticancer Activity. *Acc. Chem. Res.* **2015**, *48*, 2075−2083.

(17) Censi, V.; Caballero, A. B.; Pérez-Hernández, M.; Soto-Cerrato, V.; Korrodi-Gregório, L.; Pérez-Tomás, R.; Dell'Anna, M. M.; Mastrorilli, P.; Gamez, P. DNA-binding and in vitro cytotoxic activity of platinum(II) complexes of curcumin and caffeine. *J. Inorg. Biochem.* **2019**, *198*, 110749.

(18) Gou, M.; Men, K.; Shi, H.; Xiang, M.; Zhang, J.; Song, J.; Long, J.; Wan, Y.; Luo, F.; Zhao, X.; Qian, Z. Curcumin-loaded biodegradable polymeric micelles for colon cancer therapy in vitro and in vivo. *Nanoscale* **2011**, *3*, 1558−1567.

(19) Shutava, T. G.; Balkundi, S. S.; Vangala, P.; Steffan, J. J.; Bigelow, R. L.; Cardelli, J. A.; O'Neal, D. P.; Lvov, Y. M. Layer-by-Layer-Coated Gelatin Nanoparticles as a Vehicle for Delivery of Natural Polyphenols. *ACS Nano* **2009**, *3*, 1877−1885.

(20) Scarano, W.; de Souza, P.; Stenzel, M. H. Dual-drug delivery of curcumin and platinum drugs in polymeric micelles enhances the synergistic effects: a double act for the treatment of multidrug-resistant cancer. *Biomater. Sci.* **2015**, *3*, 163−174.

(21) Agarwal, A.; Lvov, Y.; Sawant, R.; Torchilin, V. Stable nanocolloids of poorly soluble drugs with high drug content prepared using the combination of sonication and layer-by-layer technology. *J. Controlled Release* **2008**, *128*, 255−260.

(22) Lvov, Y. M.; Pattekari, P.; Zhang, X.; Torchilin, V. Converting Poorly Soluble Materials into Stable Aqueous Nanocolloids. *Langmuir* **2011**, *27*, 1212−1217.

(23) Vergaro, V.; Civallero, M.; Citti, C.; Cosenza, M.; Baldassarre, F.; Cannazza, G.; Pozzi, S.; Sacchi, S.; Fanizzi, F.; Ciccarella, G. Cell-Penetrating $CaCO_3$ Nanocrystals for Improved Transport of NVP-BEZ235 across Membrane Barrier in T-Cell Lymphoma. *Cancers* **2018**, *10*, 31.

(24) Vergaro, V.; Papadia, P.; Leporatti, S.; De Pascali, S. A.; Fanizzi, F. P.; Ciccarella, G. Synthesis of biocompatible polymeric nanocapsules based on calcium carbonate: A potential cisplatin delivery system. *J. Inorg. Biochem.* **2015**, *153*, 284−292.

(25) Vergaro, V.; Papadia, P.; Petrini, P.; Fanizzi, F. P.; De Pascali, S. A.; Baldassarre, F.; Pastorino, L.; Ciccarella, G. Nanostructured polysaccharidic microcapsules for intracellular release of cisplatin. *Int. J. Biol. Macromol.* **2017**, *99*, 187−195.

(26) Vergaro, V.; Baldassarre, F.; De Santis, F.; Ciccarella, G.; Giannelli, G.; Leporatti, S. TGF-Beta Inihibitor-loaded Polyelectrolyte Multilayers Capsules for Sustained Targeting of Hepatocarcinoma Cells. *Curr. Pharm. Des.* **2012**, *18*, 4155−4164.

(27) Pastorino, L.; Erokhina, S.; Ruggiero, C.; Erokhin, V.; Petrini, P. Fabrication and Characterization of Chitosan and Pectin Nanostructured Multilayers. *Macromol. Chem. Phys.* **2015**, *216*, 1067−1075.

(28) Gmeiner, W. H.; Ghosh, S. Nanotechnology for cancer treatment. *Nanotechnol. Rev.* **2014**, *3*, 111−122.

(29) Santos, A. C.; Pattekari, P.; Jesus, S.; Veiga, F.; Lvov, Y.; Ribeiro, A. J. Sonication-Assisted Layer-by-Layer Assembly for Low Solubility Drug Nanoformulation. *ACS Appl. Mater. Interfaces* **2015**, *7*, 11972−11983.

(30) Shaili, E. Platinum Anticancer Drugs and Photochemotherapeutic Agents: Recent Advances and Future Developments. *Sci. Prog.* **2014**, *97*, 20−40.

(31) Zhao, J.; Hua, W.; Xu, G.; Gou, S. Biotinylated platinum(IV) complexes designed to target cancer cells. *J. Inorg. Biochem.* **2017**, *176*, 175−180.

(32) Del Coco, L.; Vergara, D.; De Matteis, S.; Mensà, E.; Sabbatinelli, J.; Prattichizzo, F.; Bonfigli, A. R.; Storci, G.; Bravaccini, S.; Pirini, F.; Ragusa, A.; Casadei-Gardini, A.; Bonafè, M.; Maffia, M.;

https://dx.doi.org/10.1021/acsabm.0c00766
ACS Appl. Bio Mater. 2020, 3, 6836−6851

Fanizzi, F. P.; Olivieri, F.; Giudetti, A. M. NMR-Based Metabolomic Approach Tracks Potential Serum Biomarkers of Disease Progression in Patients with Type 2 Diabetes Mellitus. *J. Clin. Med.* **2019**, *8*, 720.
(33) Duarte, I. F.; Ladeirinha, A. F.; Lamego, I.; Gil, A. M.; Carvalho, L.; Carreira, I. M.; Melo, J. B. Potential Markers of Cisplatin Treatment Response Unveiled by NMR Metabolomics of Human Lung Cells. *Mol. Pharm.* **2013**, *10*, 4242−4251.
(34) Moore, T. L.; Rodriguez-Lorenzo, L.; Hirsch, V.; Balog, S.; Urban, D.; Jud, C.; Rothen-Rutishauser, B.; Lattuada, M.; Petri-Fink, A. Nanoparticle colloidal stability in cell culture media and impact on cellular interactions. *Chem. Soc. Rev.* **2015**, *44*, 6287−6305.
(35) Beckonert, O.; Keun, H. C.; Ebbels, T. M. D.; Bundy, J.; Holmes, E.; Lindon, J. C.; Nicholson, J. K. Metabolic profiling, metabolomic and metabonomic procedures for NMR spectroscopy of urine, plasma, serum and tissue extracts. *Nat. Protoc.* **2007**, *2*, 2692−2703.
(36) Fan, T. W.-M. Metabolite profiling by one- and two-dimensional NMR analysis of complex mixtures. *Prog. Nucl. Magn. Reson. Spectrosc.* **1996**, *28*, 161−219.
(37) Bro, R.; Kjeldahl, K.; Smilde, A. K.; Kiers, H. A. L. Cross-validation of component models: A critical look at current methods. *Anal. Bioanal. Chem.* **2008**, *390*, 1241−1251.
(38) Antonelli, J.; Claggett, B. L.; Henglin, M.; Kim, A.; Ovsak, G.; Kim, N.; Deng, K.; Rao, K.; Tyagi, O.; Watrous, J. D.; Lagerborg, K. A.; Hushcha, P. V.; Demler, O. V.; Mora, S.; Niiranen, T. J.; Pereira, A. C.; Jain, M.; Cheng, S. Statistical Workflow for Feature Selection in Human Metabolomics Data. *Metabolites* **2019**, *9*, 143.
(39) van den Berg, R. A.; Hoefsloot, H. C.; Westerhuis, J. A.; Smilde, A. K.; van der Werf, M. J. Centering, scaling, and transformations: improving the biological information content of metabolomics data. *BMC Genom.* **2006**, *7*, 142.
(40) Chong, J.; Soufan, O.; Li, C.; Caraus, I.; Li, S.; Bourque, G.; Wishart, D. S.; Xia, J. MetaboAnalyst 4.0: towards more transparent and integrative metabolomics analysis. *Nucleic Acids Res.* **2018**, *46*, W486−W494.
(41) Parekh, G.; Pattekari, P.; Joshi, C.; Shutava, T.; DeCoster, M.; Levchenko, T.; Torchilin, V.; Lvov, Y. Layer-by-layer nanoencapsulation of camptothecin with improved activity. *Int. J. Pharm.* **2014**, *465*, 218−227.
(42) Florea, A.-M.; Büsselberg, D. Cisplatin as an anti-tumor drug: cellular mechanisms of activity, drug resistance and induced side effects. *Cancers* **2011**, *3*, 1351−1371.
(43) Gibson, D. The mechanism of action of platinum anticancer agents—what do we really know about it? *Dalton Trans.* **2009**, 10681−10689.
(44) Mitra, K.; Patil, S.; Kondaiah, P.; Chakravarty, A. R. 2-(Phenylazo)pyridineplatinum(II) catecholates showing photocytotoxicity, nuclear uptake, and glutathione-triggered ligand release. *Inorg. Chem.* **2015**, *54*, 253−264.
(45) Priya James, H.; John, R.; Alex, A.; Anoop, K. R. Smart polymers for the controlled delivery of drugs - a concise overview. *Acta Pharm. Sin. B* **2014**, *4*, 120−127.
(46) Mosmann, T. Rapid colorimetric assay for cellular growth and survival: Application to proliferation and cytotoxicity assays. *J. Immunol. Methods* **1983**, *65*, 55−63.
(47) Gökçe Kütük, S.; Gökçe, G.; Kütük, M.; Gürses Cila, H. E.; Nazıroğlu, M. Curcumin enhances cisplatin-induced human laryngeal squamous cancer cell death through activation of TRPM2 channel and mitochondrial oxidative stress. *Sci. Rep.* **2019**, *9*, 17784.
(48) Price, M.; Kessel, D. On the use of fluorescence probes for detecting reactive oxygen and nitrogen species associated with photodynamic therapy. *J. Biomed. Opt.* **2010**, *15*, 051605.
(49) Choi, Y.-M.; Kim, H.-K.; Shim, W.; Anwar, M. A.; Kwon, J.-W.; Kwon, H.-K.; Kim, H. J.; Jeong, H.; Kim, H. M.; Hwang, D.; Kim, H. S.; Choi, S. Mechanism of Cisplatin-Induced Cytotoxicity Is Correlated to Impaired Metabolism Due to Mitochondrial ROS Generation. *PLoS One* **2015**, *10*, No. e0135083.
(50) Dong, C.; Yuan, T.; Wu, Y.; Wang, Y.; Fan, T. W. M.; Miriyala, S.; Lin, Y.; Yao, J.; Shi, J.; Kang, T.; Lorkiewicz, P.; St Clair, D.; Hung, M.-C.; Evers, B. M.; Zhou, B. P. Loss of FBP1 by Snail-mediated repression provides metabolic advantages in basal-like breast cancer. *Cancer Cell* **2013**, *23*, 316−331.
(51) Del Coco, L.; Vergara, D.; De Matteis, S.; Mensà, E.; Sabbatinelli, J.; Prattichizzo, F.; Bonfigli, A. R.; Storci, G.; Bravaccini, S.; Pirini, F.; Ragusa, A.; Casadei-Gardini, A.; Bonafè, M.; Maffia, M.; Fanizzi, F. P.; Olivieri, F.; Giudetti, A. M. NMR-Based Metabolomic Approach Tracks Potential Serum Biomarkers of Disease Progression in Patients with Type 2 Diabetes Mellitus. *J. Clin. Med.* **2019**, *8*, 720.
(52) Feng, J.; Li, J.; Wu, H.; Chen, Z. Metabolic responses of HeLa cells to silica nanoparticles by NMR-based metabolomic analyses. *Metabolomics* **2013**, *9*, 874−886.
(53) Worley, B.; Powers, R. Multivariate Analysis in Metabolomics. *Curr. Metabolomics* **2012**, *1*, 92−107.
(54) Potter, M.; Newport, E.; Morten, K. J. The Warburg effect: 80 years on. *Biochem. Soc. Trans.* **2016**, *44*, 1499−1505.
(55) Chen, X.; Qian, Y.; Wu, S. The Warburg effect: evolving interpretations of an established concept. *Free Radical Biol. Med.* **2015**, *79*, 253−263.
(56) De Silva, S. S.; Payne, G. S.; Morgan, V. A.; Ind, T. E. J.; Shepherd, J. H.; Barton, D. P. J.; deSouza, N. M. Epithelial and stromal metabolite changes in the transition from cervical intra-epithelial neoplasia to cervical cancer: an in vivo 1H magnetic resonance spectroscopic imaging study with ex vivo correlation. *Eur. Radiol.* **2009**, *19*, 2041−2048.
(57) Cheng, M.; Bhujwalla, Z. M.; Glunde, K. Targeting Phospholipid Metabolism in Cancer. *Front. Oncol.* **2016**, *6*, 266.
(58) Payne, G. S.; Schmidt, M.; Morgan, V. A.; Giles, S.; Bridges, J.; Ind, T.; deSouza, N. M. Evaluation of magnetic resonance diffusion and spectroscopy measurements as predictive biomarkers in stage 1 cervical cancer. *Gynecol. Oncol.* **2010**, *116*, 246−252.
(59) Podo, F. Tumour phospholipid metabolism. *NMR Biomed.* **1999**, *12*, 413.
(60) Michel, V.; Yuan, Z.; Ramsubir, S.; Bakovic, M. Choline Transport for Phospholipid Synthesis. *Exp. Biol. Med.* **2006**, *231*, 490−504.
(61) Robinson, G. L.; Dinsdale, D.; MacFarlane, M.; Cain, K. Switching from aerobic glycolysis to oxidative phosphorylation modulates the sensitivity of mantle cell lymphoma cells to TRAIL. *Oncogene* **2012**, *31*, 4996−5006.
(62) Zand, B.; Previs, R. A.; Zacharias, N. M.; Rupaimoole, R.; Mitamura, T.; Nagaraja, A. S.; Guindani, M.; Dalton, H. J.; Yang, L.; Baddour, J.; Achreja, A.; Hu, W.; Pecot, C. V.; Ivan, C.; Wu, S. Y.; McCullough, C. R.; Gharpure, K. M.; Shoshan, E.; Pradeep, S.; Mangala, L. S.; Rodriguez-Aguayo, C.; Wang, Y.; Nick, A. M.; Davies, M. A.; Armaiz-Pena, G.; Liu, J.; Lutgendorf, S. K.; Baggerly, K. A.; Eli, M. B.; Lopez-Berestein, G.; Nagrath, D.; Bhattacharya, P. K.; Sood, A. K. Role of Increased n-acetylaspartate Levels in Cancer. *J. Natl. Cancer Inst.* **2016**, *108*, djv426.
(63) Chong, J.; Wishart, D. S.; Xia, J. Using MetaboAnalyst 4.0 for Comprehensive and Integrative Metabolomics Data Analysis. *Curr. Protoc. Bioinf.* **2019**, *68*, No. e86.
(64) Beloribi-Djefaflia, S.; Vasseur, S.; Guillaumond, F. Lipid metabolic reprogramming in cancer cells. *Oncogenesis* **2016**, *5*, No. e189.
(65) Delikatny, E. J.; Chawla, S.; Leung, D.-J.; Poptani, H. MR-visible lipids and the tumor microenvironment. *NMR Biomed.* **2011**, *24*, 592−611.
(66) Hakumäki, J. M.; Kauppinen, R. A. 1H NMR visible lipids in the life and death of cells. *Trends Biochem. Sci.* **2000**, *25*, 357−362.
(67) Vander Heiden, M. G.; Cantley, L. C.; Thompson, C. B. Understanding the Warburg Effect: The Metabolic Requirements of Cell Proliferation. *Science* **2009**, *324*, 1029−1033.

https://dx.doi.org/10.1021/acsabm.0c00766
ACS Appl. Bio Mater. 2020, 3, 6836−6851